Structural features of the inactive and active states of the melanin-concentrating hormone receptors: Insights from molecular simulations

ARTICLE *in* PROTEINS STRUCTURE FUNCTION AND BIOINFORMATICS · AUGUST 2004

Impact Factor: 2.63 · DOI: 10.1002/prot.20125 · Source: PubMed

4 AUTHORS, INCLUDING:

Pier G. De Benedetti
Università degli Studi di Modena e Reggio E…

146 PUBLICATIONS **2,876** CITATIONS

PROTEINS: Structure, Function, and Bioinformatics 56:430–448 (2004)

Structural Features of the Inactive and Active States of the Melanin-Concentrating Hormone Receptors: Insights From Molecular Simulations

Rosa Maria Vitale,[1†] Carlo Pedone,[2] Pier G. De Benedetti,[1] and Francesca Fanelli[3*]
[1]*Department of Chemistry, University of Modena and Reggio Emilia, Modena, Italy*
[2]*Istituto di Biostrutture e Bioimmagini CNR, Napoli, Italy*
[3]*Dulbecco Telethon Institute and Department of Chemistry, University of Modena and Reggio Emilia, Modena, Italy*

ABSTRACT **Comparative molecular dynamics simulations of both subtypes 1 and 2 of the melanin-concentrating hormone receptor (MCHR1 and MCHR2, respectively) in their free and hormone-bound forms have been carried out. The hormone has been used in its full-length and truncated forms, as well as in 16 mutated forms. Moreover, MCHR1 has been simulated in complex with T-226296, a novel orally active and selective antagonist. The comparative analysis of an extended number of receptor configurations suggests that the differences between inactive (i.e., free and antagonist-bound) and active (i.e., agonist-bound) states of MCHRs involve the receptor portions close to the E/DRY and NPxxY motifs, with prominence to the cytosolic extensions of helices 2, 3, 6, and 7. In fact, the active forms of these receptors share the release of selected intramolecular interactions found in the inactive forms, such as that between R3.50 of the E/DRY motif and D2.40, and that between Y7.53 of the NPxxY motif and F7.60. Another feature of the active forms of both MCHRs is the approach of "helix 8" to the cytosolic extension of helix 3. These features of the active forms are concurrent with the opening of a cleft at the cytosolic end of the helix bundle. For both MCHRs, the agonist-induced chemical information transfer from the extracellular to the cytosolic domains is mediated by a cluster of aromatic amino acids in helix 6, following the ligand interaction with selected amino acids in the extracellular half of the receptor. Proteins 2004;56:430–448.**

Key words: MCHRs; comparative Molecular Dynamics; inactive and active states; GPCRs

INTRODUCTION

Virtually any aspect of cell activity is regulated by extracellular signals that are transmitted inside the cell via different classes of plasma membrane receptors. Roughly a thousand genes of such receptors belong to the superfamily of G-protein coupled receptors (GPCRs), the largest known to date. GPCRs mediate taste, smell, vision, and the effects of most hormones and neurotransmitters.[1,2] They are also the primary site of action of many of today's life-saving drugs and the most promising target for those to be developed in the future. Mammalian GPCRs tend to fall into one of three families, termed A, B, and C.[1,2] Family A is the rhodopsin–like or adrenergic–receptor–like family; Family B is the glucagon–receptor–like or secretin–receptor–like family; and Family C is the metabotropic glutamate neurotransitter receptor family. This study is focused on subtypes 1 and 2 of the melanin-concentrating hormone receptor (MCHR1 and MCHR2, respectively) belonging to Family A, which is by far the largest and the most studied.

Despite the great biochemical and pharmacological relevance of these systems, only at the end of the year 2000 did the first detailed and unique three-dimensional (3D) structure of a GPCR, bovine rhodopsin, become available.[3]

GPCRs share a common core domain consisting of 7 transmembrane helices (TMs) connected by 3 intracellular (I1, I2, and I3) and 3 extracellular (E1, E2, and E3) loops, with the N- and C-terminal domains protruding, respectively, in the extracellular and intracellular sides of the membrane. Mutational analysis of several GPCRs has revealed that the extracellular regions and the TM domains contribute to the formation of the ligand-binding site, whereas the intracellular loops interact with G proteins, as well as with other regulatory proteins.[1,2]

A few years ago, the neuropeptide melanin-concentrating hormone (MCH) was identified as the natural ligand of an orphan GPCR homologous to the somatostatin receptors, hereafter referred to as MCHR1.[4–9] MCH, expressed predominantly in lateral hypothalamus and the zona incerta areas, is an important mediator in the regulation of the energy balance and food intake, acting as functional antagonist of α-MSH, a peptide with appetite-suppressing effect.[9] As demonstrated by experimental evidence, intracerebroventricular injection of MCH promotes feeding in

Grant sponsor: Telethon-Italy; Grant number: TCP.00068.TEL01. Grant sponsor: Compagnia S. Paolo; Grant number: TCP00068.CSP01 (to F. Fanelli).

†Permanent address: Istituto di Biostrutture e Bioimmagini CNR, Napoli, Italy

*Correspondence to: Francesca Fanelli, Dulbecco Telethon Institute and Department of Chemistry, University of Modena and Reggio Emilia, Via Campi 184, 41100 Modena, Italy. E-mail: fanelli@unimo.it

Received 8 December 2003; Accepted 9 January 2004

Published online 16 April 2004 in Wiley InterScience (www.interscience.wiley.com). DOI: 10.1002/prot.20125

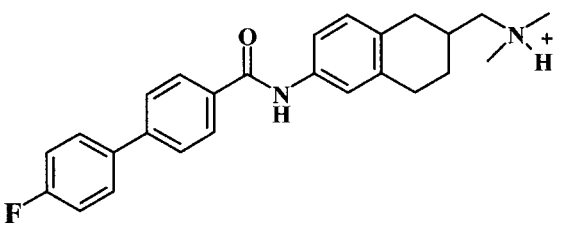

T-226296

Scheme. 1. Asp[1]-Phe[2]-Asp[3]-Met[4]-Leu[5]-Arg[6]-cyclo(S-S)(Cys[7]-Met[8]-Leu[9]-Gly[10]-Arg[11]-Val[12]-Tyr[13]-Arg[14]-Pro[15]-Cys[16])-Trp[17]-Gln[18]-Val[19]. Melanin-concentrating hormone (MCH).

mice and rats. Moreover, transgenic mice lacking the MCH gene are lean and hypophagic, with increased metabolic rates, whereas mice overexpressing the gene encoding MCH are susceptible to obesity and insulin resistance.[9,10]

At present, two MCH receptors have been identified, belonging to the rhodopsin family: the above mentioned MCHR1, isolated from rodents and humans, and MCHR2, present only in humans.[5–9,11–13] Activation of both receptors increases the levels of inositol phosphate turnover and promotes the mobilization of intracellular Ca. Moreover, MCHR1, but not MCHR2, causes the reduction of forskolin-elevated Adenosine-3′,5′-cyclic monophosphate (cAMP) levels. The amino acid sequence of MCHR2 is about 38% identical to that of MCHR1, and although its physiological role is less well understood than that of MCHR1, MCHR2 may also be involved in energy homeostasis, since it is expressed in brain regions implicated in the regulation of body weight.[9,10]

MCH is a cyclic, 19–amino acid peptide carrying a disulfide bridge between Cys7 and Cys16 (Scheme 1).[9] Recently, several studies have underlined the importance for biological activity of the MCH residues Arg6, Met8, Arg11, and Tyr13, as well as of the disulfide bridge.[14,15] Moreover, Ac-Arg[6]-cyclo(S-S)(Cys[7]-Met[8]-Leu[9]-Gly[10]-Arg[11]-Val[12]-Tyr[13]-Arg[14]-Pro[15]-Cys[16])-NH_2 (i.e., MCH6-16) has been identified as the minimal peptide length exhibiting similar agonist activity at both receptor subtypes, as compared to the full-length MCH.[15] Furthermore, site-directed mutagenesis on the MCHR1 has highlighted the amino acids on the receptor that might contribute to the hormone binding.[14] The conformational features of MCH have been recently determined by NMR spectroscopy and molecular dynamics (MD) studies.[16–18] The work by Vitale et al.[18] has shown a significant convergence of most conformers into a single fold in the 4–17 region, with a limited variability around Gly[10] and Tyr[13] on going from $CD_3CN/H_2O(10\%D_2O)$ to pure water. The main feature deduced from secondary structure analysis is the occurrence of a N-terminal α-helix of variable length, which spans an overall range of 2–9 residues. These structures are substantially different from that previously reported for the cyclic MCH5-14 portion of salmon MCH,[16,17] which has also been used to build an interaction model between MCH and MCHR1.[14]

All together, structure affinity relationships on MCHR1 and MCHR2,[14,15] the recent determination of the structure of the whole human MCH,[18] and the availability of a rhodopsin structure[3,19] homologous to MCHRs constitute the experimental background of the computational experiments done in this study. Herein, we have used the same comparative approach as that previously used to infer the structural features of mutation- and ligand-induced inactive and active forms of selected GPCRs of the rhodopsin family, including the α_{1b}-adrenergic, m3-muscarinic, oxytocin, and lutropin receptors, and, very recently, the 5-HT_{1A} serotonin receptor.[20–31] Herein, we report the results of molecular simulations of both MCHR1 and MCHR2 in their free and hormone-bound forms. The hormone has been used in its wild-type, full-length, and truncated forms, as well as in 16 mutated forms. Furthermore, MCHR1 has been also simulated in complex with T-226296, a novel, orally active and selective antagonist (Scheme 1).[32]

The results of this study provide suggestions on the amino acids responsible for the transfer of the structural changes from the agonist binding site to the G-protein coupling domains, as well on the structural features differentiating the ligand-induced active from the inactive receptor forms.

METHODS

Comparative Modeling of MCHR1 and MCHR2

The models of MCHR1 (SWISS-PROT Primary Accession Number: Q96S47) and MCHR2 (SWISS-PROT Primary Accession Number: Q969V1) were built by comparative modeling (through the MODELER 6v1 program),[33] by using two X-ray structures of bovine rhodopsin [Protein Data Bank (PDB) codes: 1F88 and 1HZX][3,19] as templates. For both receptors, the entire sequence was modeled. The majority of the MCHR1 and MCHR2 domains can, indeed, be reliably modeled based upon the homologous domains in rhodopsin structure.

For each MCHR, different alignments and modified rhodopsin templates were probed. Each MODELER run produced 50 models by randomizing the Cartesian coordinates of the model through a random number uniformly distributed in an interval from −4 Å to 4 Å.[33] For each receptor, one model was finally selected that showed one of the lowest violations of stereochemical restraints (i.e., low value of the Objective Function)[33] associated with one of the highest values of 3D-Profile score, computed by means of the Protein Health module in the QUANTA 2000 package (www.accelrys.com). The two alignments used for building the finally selected models of MCHR1 and MCHR2 are reported in Figures 1 and 2. To achieve the final model of MCHR1, the rhodopsin structure codified as 1F88 was subjected to deletions of the following amino acid segments: 230–235 and 240–242 (both from I3), as well as 323–327 and 334–348 (both from the C-tail); on the other hand, the rhodopsin structure codified as 1HZX was subjected to the following amino acid deletions: 230–235 and 241–244 (both from I3). For achieving the final model of MCHR2, the amino acid segments 240–242 (from I3), as well as 323–327 and 334–348 (both from the C-tail), were deleted in 1F88, whereas the amino acid stretch 241–244

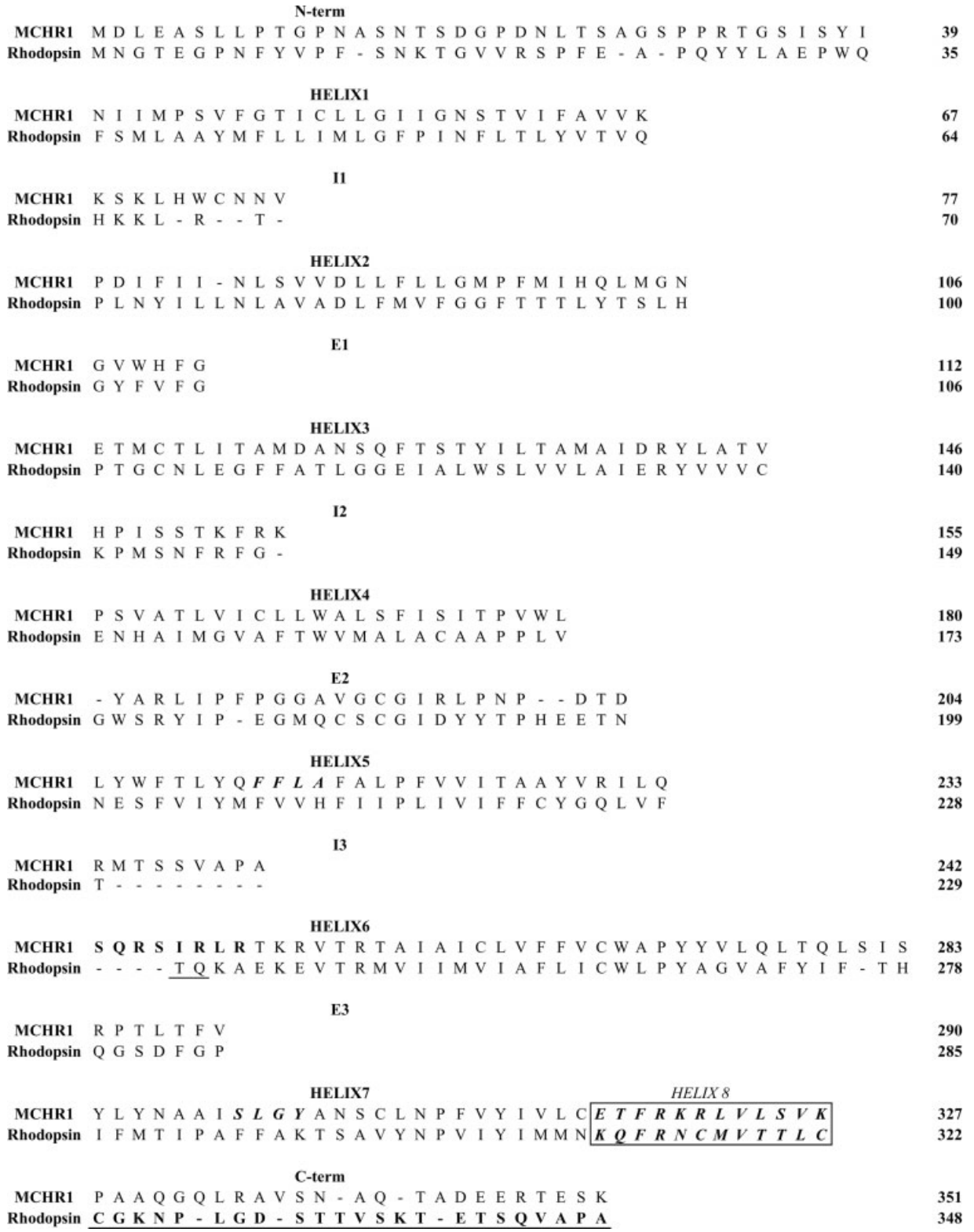

Fig. 1. Sequence alignment between rhodopsin and the human MCHR1. Both rhodopsin structures encoded as 1F88[3] and 1HZX[19] have been employed as templates, following some deletions. In detail, 1F88 has been subjected to deletions of the following amino acid segments: 230–235 and 240–242 (both from I3), as well as 323–327 and 334–348 (both from the C-tail); on the other hand, 1HZX has been subjected to the following amino acid deletions: 230–235 and 241–244 (both from I3). In this respect, the underlined sequence at the beginning of rhodopsin's helix 6 has been deleted in 1HZX and not in 1F88. On the contrary, the C-tail has been deleted in 1F88 and not in 1HZX (sequence in bold text underlined). The bold sequence at the beginning of helix 6 in MCHR1 has been subjected to α-helical restraints by MODELER. The amino acids, which belong to "helix 8" (at the end of helix 7), are highlighted in bold italics and boxed both in MCHR1 and rhodopsin sequences. Moreover, the amino acid stretches found in noncanonical α-helical conformation in the input structure of MCHR1 are in bold italics, both in MCHR1 and rhodopsin sequences.

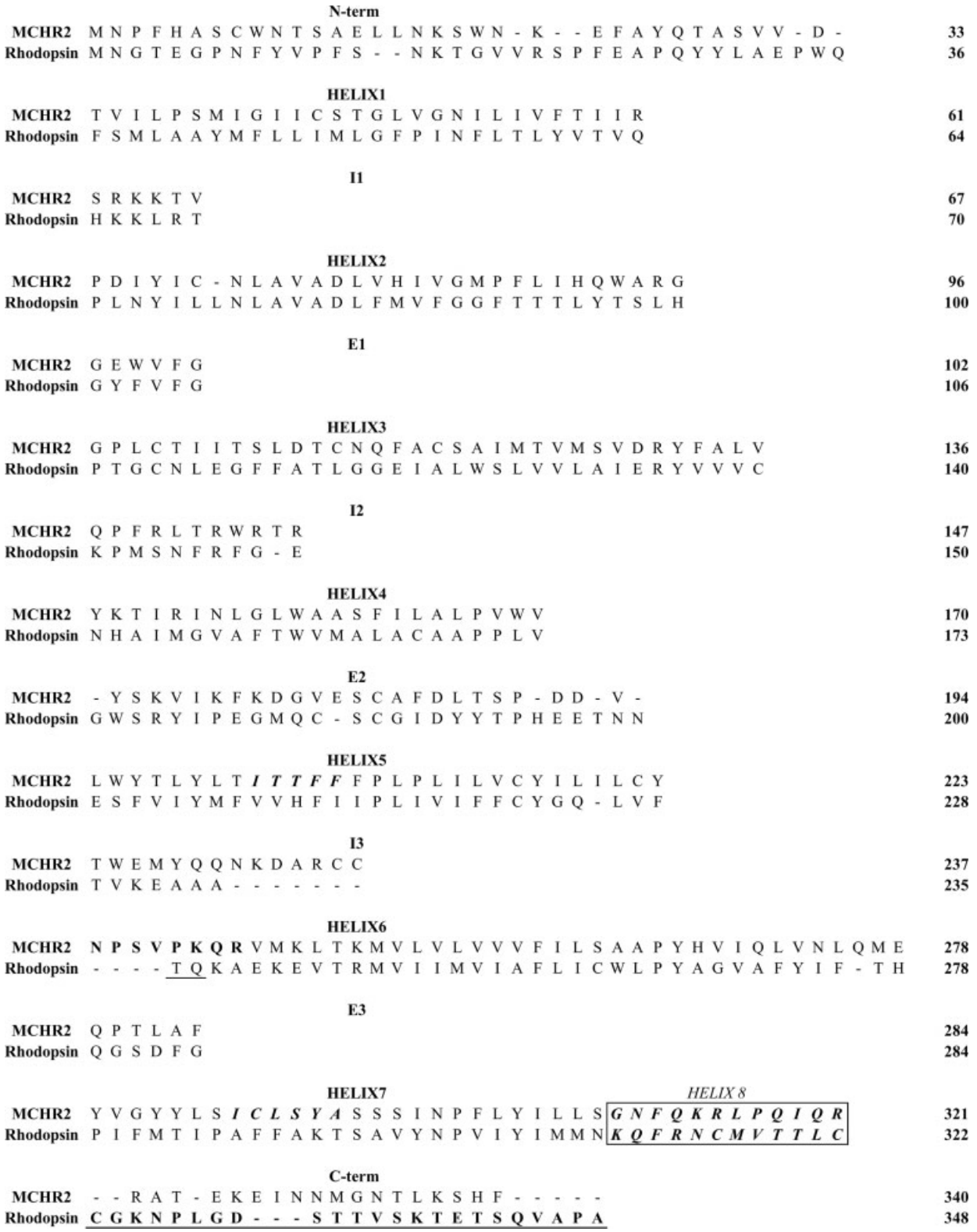

Fig. 2. Sequence alignment between rhodopsin and the human MCHR2. Both rhodopsin structures encoded as 1F88[3] and 1HZX[19] have been employed as templates, following some deletions. In detail, 1F88 has been subjected to deletions of the following amino acid segments: 240–242 (from I3), as well as 323–327 and 334–348 (both from the C-tail); on the other hand, 1HZX has been subjected to the following amino acid deletions: 241–244 (from I3). In this respect, the underlined sequence at the beginning of rhodopsin's helix 6 has been deleted in 1HZX and not in 1F88. On the contrary, the C-tail has been deleted in 1F88 and not in 1HZX (sequence in bold and underlined). The bold sequence at the beginning of helix 6 in MCHR2 has been subjected to α-helical restraints by MODELER. The amino acids, which belong to "helix 8" (at the end of helix 7) are highlighted in bold italic and are boxed, both in MCHR2 and rhodopsin sequences. Moreover, the amino acid stretches found in noncanonical α-helical conformation in the input structure of MCHR2 are in bold italics.

(from I3) was deleted in 1HZX. The MCHR1 243–250 segment and the MCHR2 238–245 segment, which constitute the cytosolic extensions of helix 6, were subjected to α-helical restraints during the model building by MODELER (bold characters in Figures 1 and 2).[33]

Molecular Dynamics Simulations

The finally selected models of the two MCHRs were subjected to automatic and manual rotation of the side-chain torsion angles when in nonallowed conformations. Respectively, 11 and 8 input arrangements of the empty MCHR1 and MCHR2, differing in the conformation of a few amino acids, were subjected to energy minimization and MD simulations by CHARMM 27, by using the "all atom" representation.[34,35] Since, for both receptor models, the starting conformation and orientation of the C-tail might be low reliable, such domains have been deleted from the structures selected for calculations. To take into account, at least in part, the lack of the C-tail, the backbone carboxy-function of the last amino acid was *N*-methylamidated during minimization and MD simulations. Minimizations were carried out by using 1500 steps of steepest descent followed by a conjugate gradient minimization, until the root-mean-square gradient was less than 0.001 kcal/mol Å. A distance-dependent dielectric term ($\epsilon = 4r$) was chosen. MD simulations were carried out on the minimized coordinates of MCHRs in their free and ligand-bound forms. The lengths of the bonds involving the hydrogen atoms were constrained according to the SHAKE algorithm, allowing for an integration timestep of 1 fs. The systems were heated to 300 K, with 7.5 K rise every 2.5 ps per 100 ps, by randomly assigning velocities from the Gaussian distribution. After heating, the system was allowed to equilibrate for 50 ps.

A disulphide bridge patch was applied between (1) C116(3.25) and C194 (in E2) for MCHR1; (2) C106(3.25) and C184 (in E2) for MCHR2; and (3) Cys7 and Cys16 for the hormone MCH. For the amino acids in the receptor helix bundle, the numbering from Ballesteros and Weinstein is also reported in parenthesis.[36] Concerning such arbitrary numbering, the α-helical segment corresponding to the rhodopsin's helix 8 (i.e., herein indicated as "helix 8," Figs. 1 and 2) is considered as a cytosolic extension of helix 7. Moreover, the one-letter code has been employed for the amino acids in the receptor, whereas the three-letter code has been employed for the amino acids that constitute the hormone.

The secondary structure of the helix bundle was preserved by assigning distance restraints (i.e., minimum and maximum allowed distances of 2.7 Å and 3.0 Å, respectively) between the backbone oxygen atom of residue i and the backbone nitrogen atom of residue $i+4$. The application of these intrahelical distance restraints was instrumental in (1) reducing the system degrees of freedom, (2) inferring the structural/dynamics role of prolines, which are not involved in such restraints, and (3) letting the helices move as rigid bodies, consistent with the experimental evidences on rhodopsin activation.[37]

For the empty receptor forms, short (100 ps) equilibrated MD runs were carried out, probing different input structures and different combinations of intrahelical distance restraints. The latter tests consisted of applying distance restraints to different amino acid stretches in each helix. Finally, the computation conditions and the input receptor structure were chosen, which, following MD simulation, produced average arrangements characterized by a good quality (evaluated by means of the Protein Health module in the QUANTA 2000 package), together with structural similarity to rhodopsin. The similarity between the average minimized structures of the empty MCHRs and rhodopsin structure was evaluated based upon the root-mean-square deviation (RMSD) of the main-chain backbone atoms in the transmembrane domains, as well as the degree of conservation of the interaction patterns involving the conserved amino acids.

The finally selected intrahelical distance restraints involved the following amino acid stretches: For the MCHR1: (1) 38–66 in helix 1, (2) 78–106 in helix 2, (3) 113–145 in helix 3, (4) 158–180 in helix 4, (5) 205–232 in helix 5, (6) 246–280 in helix 6, (7) 291–314 in helix 7, and (8) 315–327 in "helix 8". For the MCHR2: (1) 35–61 in helix 1, (2) 68–96 in helix 2, (3) 103–135 in helix 3, (4) 147–169 in helix 4, (5) 196–219 in helix 5, (6) 244–276 in helix 6, (7) 288–310 in helix 7, and (8) 310–321 in "helix 8."[3,19] For both receptors, the backbone oxygen atoms of the amino acids at position $i-4$ with respect to prolines were not subjected to distance restraints. Furthermore, the backbone carbonyl oxygen atoms of the amino acids at positions 81 and 82 in MCHR1, and at positions 71 and 72 in MCHR2, were restrained to make H-bond with the backbone nitrogen atom at position $i+3$. This has been done due to the noncanonical α-helix conformation involving, in the starting structures of the two MCHRs, the amino acids just before and after the deletion in helix 2, in the selected sequence alignments between rhodopsin and MCHRs (Figs. 1 and 2). However, the noncanonical α-helical conformation in such portions of helix 2 always moves onto a canonical one, following MD simulations. On the same line, the backbone oxygen atoms of the amino acid stretches 213–216 and 203–207 in helix 5 of MCHR1 and MCHR2, respectively (i.e., italicized characters in Figs. 1 and 2), were not subjected to distance restraints or subjected to distance restraints with the backbone nitrogen atoms at position $i+5$. Furthermore, the backbone oxygen atoms of the amino acid stretches 298–301 and 292–297 in helix 7 of MCHR1 and MCHR2, respectively (i.e., italicized characters in Figs. 1 and 2), were not subjected to distance restraints or subjected to distance restraints with the backbone nitrogen atoms at position $i+3$. These conditions allowed us to better account for the irregularities in the α-helical conformation in the extracellular halves of helices 5 and 7, as inherited from rhodopsin structure. These conditions of intrahelical distance restraints were used also for relatively long (2 ns) MD simulations of the empty receptors.

The selected MCHR1 and MCHR2 input structures show RMSDs of 0.30 Å and 0.28 Å, respectively, from rhodopsin structure. RMSDs were computed by superim-

posing the main-chain atoms of segments 39–62, 78–99, 111–133, 152–171, 203–223, 253–276, and 286–306, representing the 7 transmembrane domains of rhodopsin, with those in the homologous segments 42–65, 84–106, 117–139, 159–178, 208–228, 257–280, and 291–311 of MCHR1 and 36–59, 74–96, 107–129, 149–168, 197–217, 252–275, and 286–306 of MCHR2 models. This deviation increased on average 1.00 Å following energy minimizations and MD simulations, approaching the expected values (i.e., between 1.5 Å and 2.2 Å), considering that the sequence identity is 20.7% and 22.6%, respectively, between the matched segments of rhodopsin, on one side, and of MCHR1 and MCHR2, on the other.[38]

The computation conditions and the input structure selected, based upon MD simulations of the empty MCHR1 and MCHR2, were used for simulating the ligand–receptor complexes following manual docking of the agonist MCH in both receptors and of the antagonist T-226296 only in MCHR1 (Scheme 1). The key interaction considered for driving the initial orientation of MCH into the binding sites of MCHR1 and MCHR2 was the charge reinforced H-bond between Arg11 and D3.32, according to the experimental evidence.[14] The approach between the functionally important Tyr13 of the hormone[14,15] and Y6.51 of the receptor was additionally considered in manual docking, based upon indirect experimental evidences on the agonist-induced α_{1b}-adrenergic receptor (α_{1b}-AR) activation.[39] The charge-reinforced H-bond between the protonated nitrogen atom of T-226296 and D3.32 was used to drive the docking of the antagonist into the MCHR1 binding site based upon experimental evidence on the binding of cationic ligands at their cognate receptors, including MCHRs.[2,14,40]

The employed structure of the natural agonist MCH was extracted from one of the clusters of structures recently achieved by NMR.[18] For MCHR1 and MCHR2, respectively, 121 and 45 different hormone–receptor complexes were probed by MD, which differed in the orientation of the ligand and in the conformation of the ligand and/or of the receptor side-chains. For the tests, MD production phases of 100 ps were employed, analyzing the structures averaged over the 200 structures collected in each equilibrated MD run and minimized. The input structures of the complexes, which led to average arrangement characterized by good quality (as checked by means of the Protein Health module in the QUANTA 2000 package) and consistency with the available experimental data (see the Results section),[14,15] were used for generating 2 ns trajectories.

Minimizations and MD simulations were carried out on a 12 processor AMD Athlon 1000 Linux Cluster and on a biprocessor AMD Athlon MP 2000+.

The structure of the antagonist T-226296 (Scheme 1),[32] built by means of the QUANTA 2000 package in its protonated form, was optimized through semiempirical Molecular Orbitals (MO) calculations (AM1) within the MOPAC 6.0 suite of programs.[41] Twenty-one different initial configurations of the antagonist–receptor complex were probed by MD. These complexes differed for the orientation of the ligand and/or the conformation of the ligand and the receptor side-chains. Different conditions of distance restraints were probed between the cationic nitrogen atom of the ligand and the carboxy-carbon atom of D123(3.32). Simulations were also done by associating such restraints with distance restraints between the carbonyl-oxygen atom of the ligand and the side-chain nitrogen atom of Q212(5.42). The latter restraints were assigned because, in the input structure, Q212(5.42) is close to the carbonyl-oxygen atom of the ligand and is one of the few polar amino acids in the putative ligand-binding site, which is not present in the MCHR2 that does not bind the antagonist.[32] For some antagonist–receptor complexes, MD runs without using intermolecular distance restraints were also done. Tests were done using short MD runs. Those input complexes that produced average arrangements characterized by the best accomplishment of the charge reinforced H-bond between the protonated nitrogen atom of the ligand and D123(3.32), together with an overall good ligand–receptor complementarity, were subjected to relatively long (2 ns) MD runs.

The truncated MCH6-16 peptide was obtained by deleting the amino acid stretches 1–5 and 17–19 from the selected structure of the full-length peptide. This peptide was docked into both MCHR1 and MCHR2 exactly in the same conformation and orientation as that of the full-length peptide in the selected starting complexes with each receptor subtype. The N- and C-termini of the truncated peptide were, respectively, acetylated and amidated during calculations. The input structures of the complexes between the mutated MCH and both MCHR1 and MCHR2 were obtained by mutating each targeted amino acid in the selected complexes between the wild-type MCH and each receptor subtype.

The complexes between either MCHR1 or MCHR2 and either the truncated or the mutated forms of MCH were subjected to MD production phases of 100 ps.

RESULTS

Comparative MD simulations of both the MCHR1 and MCHR2 subtypes in their free and hormone-bound forms have been carried out. The hormone has been used in its full-length and truncated forms, as well as in 16 mutated forms. Moreover, MCHR1 has been simulated in complex with T-226296,[32] a novel orally active and selective antagonist (Scheme 1).

The approach consists of comparative analyses of a large number of short (100 ps) and relatively long (2 ns) MD trajectories, probing different starting structures, as well as different intrahelical (for the empty receptor form) and intermolecular (for the antagonist-bound forms) distance restraints. In particular, the following numbers of equilibrated MD runs have been carried out for MCHR1: (1) 11 short and 6 long for the empty receptor, (2) 106 short and 15 long for the MCH–receptor complexes, and (3) 16 short and 5 long for the antagonist–receptor complexes. As for MCHR2, the following numbers of equilibrated MD runs have been carried out: (1) 1 short and 7 long for the empty

receptor, and (2) 44 short and 1 long for the MCH–receptor complex.

For the empty MCHR1 and MCHR2 receptors, the criteria for selecting the short trajectories that could be worth prolonging included the quality of the average minimized structures and their degree of similarity to rhodopsin structure (see the Methods section). For the MCH–receptor complexes, the criteria for selecting the trajectories that could be worth prolonging included the quality of the average minimized structures and their consistency with the results of site-directed mutagenesis experiments coupled with binding and functional assays on the two MCHRs, as well as on other GPCRs.[2,14,15,39,40] For the antagonist–receptor complex, the major criterion was the accomplishment of the charge-reinforced H-bond between the protonated nitrogen atom of the ligand and D123(3.23) of the receptor. In fact, this aspartate has been demonstrated to be essential for the agonist binding at the MCHR1.[14] Moreover, an aspartate at the homologous position has been demonstrated to be essential for both cationic agonist and antagonist binding at homologous GPCRs, including the α_{1b}-AR.[2,40]

The mechanistic hypothesis inferred from this study is based upon the outcome of all the short and long MD runs that have been carried out. However, herein, only one rather representative long trajectory for each of the different forms of MCHR1 (i.e., free, antagonist-bound, and agonist-bound) and of MCHR2 (i.e., free and agonist-bound) will be shown.

MD Simulations of the Empty and Antagonist-Bound Forms of MCHR1: Structural Features of the Inactive States

In the selected 2 ns trajectory of the empty MCHR1, R141(3.50) of the E/DRY motif is involved in persistent charge reinforced H-bonding interactions with both D79(2.40) and the adjacent D140(3.49) (Table I, Figure 3). The former interaction is a peculiarity of MCHR1, whereas the latter is homologous to the interaction that has been found in all the rhodopsin structures resolved so far.[3,19,42] Moreover, these interactions characterize the majority of the empty MCHR1 structures collected over the other long trajectories produced from different input arrangements (results not shown). The other highly conserved amino acids in helices 2, 4, 6, and 7 perform the following interactions, selected among the most persistent ones over the 2 ns trajectory (Table I):

1. D89(2.50) is involved in H-bonds with both S304(7.46) and N307(7.49), and in van der Waals attractive interactions with N58(1.50).
2. W168(4.50) is involved in interhelical van der Waals attractive interactions with both N84(2.45) and I133(3.42), and intrahelical interactions with I164(4.46). A similar interaction between the tryptophan at position 4.50 and the asparagine at position 2.45 characterizes the dark state of rhodopsin.[3,19,42]
3. F265(6.44) performs interhelical van der Waals attractive interactions with T131(3.40) and N303(7.45), and intrahelical orthogonal σ-π interactions with W269(6.48).
4. W269(6.48) performs interhelical van der Waals attractive interactions with Q127(3.36) and H-bond with N303(7.45), as well as intrahelical orthogonal σ-π interactions with both F265(6.44) and Y272(6.51).
5. N307(7.49), of the NPxxY motif, is persistently involved in H-bond with D89(2.50), being involved in additional intrahelical H-bond with N303(7.45) in the second half of simulation.
6. Finally, Y311(7.53) makes almost persistent van der Waals attractive interactions with V61(1.53), I83(2.44), L85(2.46), T256(6.36) and F318(7.60).

The interaction pattern of W268(6.48) is similar to that found in rhodopsin structures.[3,19,42] In fact, similar to rhodopsin structure, it interacts with both F6.44 and Y6.51, forming a cluster of aromatic amino acids in helix 6. Furthermore, similar to rhodopsin, it is oriented toward the polar amino acid at position 7.45 [i.e., an asparagine in MCHR1 and a serine in rhodopsin (Figs. 1 and 3)]. This arrangement of the aromatic cluster in helix 6 is associated with a bend at P271(6.50), similar to rhodopsin structures (Fig. 3).[3,19,42]

As for the antagonist-bound forms of MCHR1, in all the simulated complexes between T-226296 and MCHR1, the antagonist docks into a site essentially formed by amino acids in helices 3, 4, 5, 6, and 7 (Fig. 3). The main axis of the quite rigid ligand is almost parallel to the putative membrane surface, the ligand being oriented in such a way that its protonated head group docks in between helices 3 and 7, whereas the diphenyl moiety docks in between helices 4 and 5 (Fig. 3). In the selected trajectory of the antagonist–receptor complex, which is representative of the most populated docking modes of such a ligand, the protonated nitrogen atom of the ligand performs a persistent charge-reinforced H-bond with D123(3.32) (Fig. 3). This is also due to the distance restraints (i.e., minimum and maximum allowed distances of 2.5 Å and 3.0 Å, respectively) that have been imposed during MD simulations between the protonated nitrogen atom of the ligand and the carboxy-carbon atom of D123(3.32). The importance of such interaction for the binding of T-226296 at the MCHR1 has been inferred from indirect experimental evidences.[2,14,40] Other intermolecular interactions that frequently characterize the antagonist–receptor complexes, include van der Waals attractive interactions between the dimethyl-amino moiety of the ligand and both Y272(6.51) and I297(7.39) of the receptor (Fig. 3). Furthermore, in the first half of the selected 2 ns trajectory, a weak and nonpersistent H-bond occurs between the carbonyl-oxygen atom of the ligand and Q212(5.42). The second half of the trajectory is characterized by the strengthening of van der Waals attractive interactions between (1) the fluorine atom of the ligand and I173(4.55), and (2) the tetrahydro-naphthalene ring of the ligand and both V178(4.60) and F208(5.38) (Scheme 1, Fig. 3). Such a docking mode of the antagonist is associated with persistent charge-reinforced H-bonds between R141(3.50) and

TABLE I. Intramolecular Interactions Involving Selected Amino Acid Side-Chains and Theoretical Indices Computed on the Average Minimized Structures of MCHR1

MCHR1	D89(2.50)[e]	D140(3.49)[e]	R141(3.50)[e]	N307(7.49)[e]	Y311(7.53)[e]	SAS1[f]
$FREE_{f100ps}$[a]	N58(1.50)	**R141(3.50)**	I82(2.43)	**D89(2.50)**	V61(1.53)	9.0
	N303(7.45)	**K153**	**D79(2.40)**	I261(6.40)	I83(2.44)	
	S304(7.46)		**D140(3.49)**	N303(7.45)	T257(6.36)	
	N307(7.49)		T251(6.30)		F318(7.60)	
			V254(6.33)			
$FREE_{f1000ps}$[b]	N58(1.50)	**R141(3.50)**	I82(2.43)	**D89(2.50)**	V61(1.53)	15.0
	S304(7.46)	**K153**	**D79(2.40)**	I261(6.40)	I83(2.44)	
	N307(7.49)		**D140(3.49)**	N303(7.45)	L85(2.46)	
			T251(6.30)		F318(7.60)	
			V254(6.33)			
$FREE_{l1000ps}$[c]	N58(1.50)	**R141(3.50)**	I82(2.43)	**D89(2.50)**	I83(2.44)	36.0
	S304(7.46)	**K153**	**D79(2.40)**	**N303(7.45)**	L85(2.46)	
	N307(7.49)		**D140(3.49)**		F318(7.60)	
			T251(6.30)			
			V254(6.33)			
$FREE_{l100ps}$[d]	N58(1.50)	**R141(3.50)**	I82(2.43)	**D89(2.50)**	I83(2.44)	23.0
	S304(7.46)		**D79(2.40)**	**N303(7.45)**	L85(2.46)	
	N307(7.49)		**D140(3.49)**		F318(7.60)	
			T251(6.30)			
			V254(6.33)			
ANTA-$bound_{f100ps}$[a]	N58(1.50)	**R141(3.50)**	I82(2.43)	**D89(2.50)**	V61(1.53)	16.0
	S130(3.39)	**K153**	**D79(2.40)**	I261(6.40)	I83(2.44)	
	S304(7.46)		**D140(3.49)**	N303(7.45)	M137(3.46)	
	N307(7.49)		T251(6.30)		F318(7.60)	
			V254(6.33)			
ANTA-$bound_{f1000ps}$[b]	N58(1.50)	**R141(3.50)**	I82(2.43)	**D89(2.50)**	V61(1.53)	8.0
	S130(3.39)	**K153**	**D79(2.40)**	I261(6.40)	I83(2.44)	
	S304(7.46)		**D140(3.49)**	N303(7.45)	M137(3.46)	
	N307(7.49)		T251(6.30)		F318(7.60)	
			V254(6.33)			
ANTA-$bound_{l1000ps}$[c]	N58(1.50)	**R141(3.50)**	I82(2.43)	**D89(2.50)**	V61(1.53)	6.0
	S130(3.39)	**K153**	**D79(2.40)**	I261(6.40)	I83(2.44)	
	S304(7.46)		**D140(3.49)**	N303(7.45)	M137(3.46)	
	N307(7.49)		T251(6.30)		F318(7.60)	
			V254(6.33)			
ANTA-$bound_{l100ps}$[d]	**N58(1.50)**	**R141(3.50)**	I82(2.43)	N58(1.50)	V61(1.53)	0.0
	S130(3.39)	**K153**	**D79(2.40)**	D89(2.50)	I83(2.44)	
	S304(7.46)		**D140(3.49)**	I261(6.40)	M137(3.46)	
	N307(7.49)		T251(6.30)		F318(7.60)	
			V254(6.33)			
MCH-$bound_{f100ps}$[a]	**N125(3.34)**	**R141(3.50)**	**D140(3.49)**	I261(6.40)	I133(3.42)	167.0
	S126(3.35)	**K153**	A144(3.53)	**N303(7.45)**	L134(3.43)	
	T129(3.40)		V254(6.33)	Y311(7.53)	I261(6.40)	
MCH-$bound_{f1000ps}$[b]	**N125(3.34)**	**N76**	D140(3.49)	I261(6.40)	I133(3.42)	184.0
	S126(3.35)	R141(3.50)		N303(7.45)	L134(3.43)	
					I261(6.40)	
MCH-$bound_{l1000ps}$[c]	**N125(3.34)**	N76	N76	I261(6.40)	I133(3.42)	178.0
	S126(3.35)	R141(3.50)	D140(3.49)	Y311(7.53)	L134(3.43)	
	T129(3.40)	**K153**			N307(7.49)	
MCH-$bound_{l100ps}$[d]	**N125(3.34)**	N76	**D140(3.49)**	I261(6.40)	I133(3.42)	254.0
	T129(3.40)	**R141(3.50)**	A144(3.53)	Y311(7.53)	L134(3.43)	
			V254(6.33)		N307(7.49)	
			T317(7.59)			

[a]Structures of the free (FREE), antagonist-bound (ANTA-bound), and agonist-bound (MCH-bound) forms of MCHR1, averaged over the 200 configurations collected during the first 100 ps of the selected 2 ns trajectories and minimized.
[b]Structures of the FREE, ANTA-bound, and MCH-bound forms of MCHR1, averaged over the 2000 configurations collected during the first 1000 ps of the selected 2 ns trajectories and minimized.
[c]Structures of the FREE, ANTA-bound, and MCH-bound forms of MCHR1, averaged over the 2000 configurations collected during the last 1000 ps of the selected 2 ns trajectories and minimized.
[d]Structures of the FREE, ANTA-bound, and MCH-bound forms of MCHR1, averaged over the 200 configurations collected during the last 100 ps of the selected 2 ns trajectories and minimized.
[e]Amino acids involved in the selected intramolecular interactions. H-bonding interactions between the side-chain atoms are highlighted in bold.
[f]Solvent accessible surface area ($Å^2$) computed over N76(2.37), R141(3.50), K153 (in I2), I247(6.26), and T251(6.30).

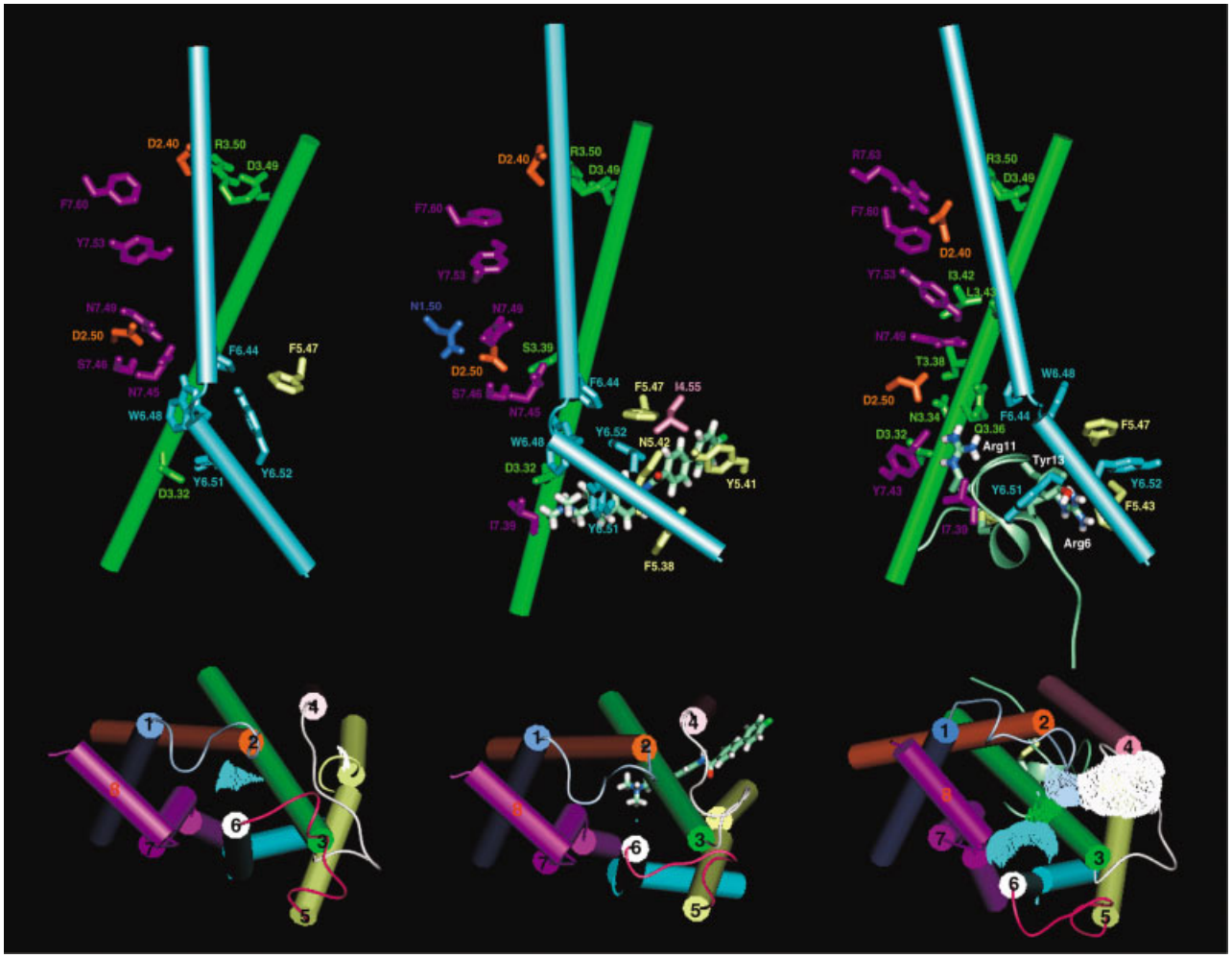

Fig. 3. Structures of the empty (**top and bottom left**), antagonist-bound (**top and bottom middle**), and MCH-bound (**top and bottom right**) forms of MCHR1 averaged over the 200 structures collected during the last 100 ps of the selected 2 ns trajectories and minimized. Helices 1, 2, 3, 4, 5, 6, and 7 are, respectively, colored blue, orange, green, pink, yellow, cyan, and violet, whereas the intracellular loops 1, 2, and 3 are colored in gray, white, and purple, respectively. The amino acids are labeled according to the numbering scheme proposed by Ballesteros and Weinstein.[36] **Top view:** The models are viewed in a direction parallel to the membrane surface, the cytosolic side being at the top. Only helices 3 and 6 are shown, represented by cylinders. Details of selected intramolecular and intermolecular interactions are shown. The antagonist is represented by sticks, whereas MCH is represented by cartoons. **Bottom view:** The 7-helix bundle (represented by cylinders) and the 3 intracellular loops are shown from the intracellular side in a direction perpendicular to the membrane surface. The solvent-accessible surface computed over N76(2.37), R141(3.50), K153 (in I2), I247(6.26), and T251(6.30) is represented by dots colored according to the color of the corresponding amino acid.

both D79(2.40) and D140(3.49), similar to the empty receptor forms (Table I and Fig. 3). On the same line, in the majority of the antagonist–MCHR1 complexes, the other conserved amino acids in helices 2, 6, and 7 perform intramolecular interactions almost comparable with those found in the empty receptor form (Table I, Fig. 3). Similar to the empty receptor, the arrangement of the aromatic cluster in helix 6 is concurrent with a significant bend at P271(6.50) (Fig, 3).

MD Simulations of the Agonist-Bound Forms of MCHR1: Structural Features of the Active States

In almost all the MCH–MCHR1 complexes collected during the 106 short and 15 long MD simulations, the hormone docks into a site formed by amino acids in helices 3, 4, 5, 6, and 7, as well as in E2. In particular, (1) the main-chain of the N-terminal segment (i.e., segment 1–6) docks into a site formed by amino acids in helices 5 and 6, and in E2; (2) the main-chain of the cyclic peptide (i.e., segment 7–16) essentially docks into a site formed by amino acids in helices 3, 4, 5, 6, and 7, and in E2; and (3) the C-terminal linear peptide (i.e., segment 17–19) docks on the outer faces of helices 3 and 4 (Fig. 3).

Some of the most relevant (according to the experimental evidence)[14,15] and persistent intermolecular interactions are listed as follows:

1. In the first 100 ps, Arg6 is involved in van der Waals attractive interactions with both F213(5.43) and Q276(6.55). The former interaction is retained over the entire simulation time, whereas the latter is lost in the first half of simulation.

2. Met8 is involved in almost persistent van der Waals attractive interactions with both I196 and R197 (in E2).
3. Arg11 is involved in charge-reinforced H-bond with D123(3.32), H-bond with Q127(3.36), and van der Waals attractive interactions with both I297(7.39) and Y301(7.43) (Fig. 3).
4. Tyr13, in the first steps, is involved in π-π coplanar interaction with W269(6.48) and in van der Waals attractive interactions with Y272(6.51) and Q276(6.55). This interaction pattern is almost maintained during the whole simulation time, the interaction between Tyr13 and W269(6.48) being lost in the second half of simulation. The nature of the interaction between Tyr13 and Q276(6.55) is H-bonding almost persistently over the last 1500 steps of the equilibrated 2 ns trajectory (Fig. 3). In other trajectories, Tyr13 interacts with Y272(6.51) in the early steps and with W269(6.48) in the remaining time of simulation, in which Y272(6.71) can be found involved in H-bonding interaction with Arg11 (results not shown).

The arrangement of helices 1, 2, 3, 4, 6, and 7 in the MCH–MCHR1 complexes is different from that of the empty and antagonist-bound receptor forms (Fig. 3). In particular, (1) helix 3 undergoes an outward motion, being less tilted and slightly shifted toward the cytosol; (2) the outward motion of helix 3 is concurrent with outward shifts of helices 2 and 4; (3) helices 2 and 7 move apart significantly; (4) helix 6 is shifted toward the cytosol, being slightly away from the core of the helix-bundle at its cytosolic end and less bent at P271(6.50); and, finally, (5) the main axis of "helix 8" is less parallel to the putative membrane surface, approaching the cytosolic end of helix 3. The differences in the helix arrangements in the inactive and active forms of MCHR1 are concurrent with differences in the interaction patterns of the highly conserved amino acids in the helix-bundle. In particular, markers of the changes in helix1–helix2, helix 2–helix 3, helix 2–helix 4, and helix 2–helix 7 packing interactions are the establishment of interactions between D89(2.50) and both N125(3.35) and T129(3.40), and the lack of the interactions, found in the empty and antagonist-bound forms, between (1) D79(2.40) and R(3.50) of the E/DRY motif, (2) N84(2.45) and W168(4.50), and (3) D89(2.50) on one side and N58(1.50), S304(7.46), and N307(7.49) on the other (Table I, Fig. 3). The reduction of the bend in helix 6 is related, at least in part, to the shift of the side-chain of W269(6.48) from helix 7 to helix 5, concurrent with the loss of the H-bonding interaction found in the empty and antagonist-bound forms, between W269(6.48) and N302(7.45) and the gain of the orthogonal σ-π interaction between the conserved tryptophan and F217(5.47) (Fig. 3). Moreover, such structural changes in helix 6 are concurrent with a shift of C268(6.47) from the putative membrane space toward the core of the helix-bundle, consistent with the inferences of fluorescence experiments on agonist-induced β_2-adrenergic receptor (β_2-AR) activation, which targeted the homologous cysteine.[43] Finally, the movement of "helix 8" is concurrent with changes in the interaction pattern of the NPxxY motif. In fact, in the agonist–receptor complexes, the van der Waals attractive interaction found in the empty receptor between Y311(7.53) and F318(7.60) is weakened, the tyrosine of the NPxxY motif being engaged in van der Waals attractive interactions with I133(3.42), L134(3.43), I261(6.40), and N307(7.49) (Table I, Fig. 3). Moreover, R321(7.63) performs a salt bridge with D79(2.40), approaching the cytosolic extension of helix 3. The majority of the MCH–MCHR1 complexes that constitute the 15 different relatively long trajectories, are characterized by the opening of a solvent-accessible crevice in between I2 and the cytosolic ends of helices 2, 3, and 6. This effect is accounted for by the increased solvent accessibilities, as compared to the empty and antagonist-bound forms, of selected amino acids in the cytosolic domains. Indeed, the solvent-accessible surface area computed over N76(2.37), R141(3.50), K153 (in I2), I247(6.26), and T251(6.30) (i.e., **SAS1**, Table I) is persistently below 100 Å^2, most frequently close to 0 Å^2, in the majority of the empty and antagonist-bound forms, and significantly above that value in the majority of the MCH–MCHR1 complexes produced over all the 2 ns trajectories (Figs. 3 and 4).

Consistent with the experimental data,[15] MCH6-16, the truncated form of the hormone, which has been shown to be the minimal sequence able to produce full MCHR1 activation, is able to produce average arrangements of the highly conserved amino acids similar to those that characterize the full-length MCH. This is due, at least in part, to the establishment of both the charge-reinforced H-bond between Arg11 and D123(3.32) and coplanar π-π interactions between Tyr13 and W269(6.48). These features are concurrent with a **SAS1** index above 100 Å^2, similar to the complex between MCHR1 and the full-length MCH (Table II).

Molecular simulations of the complexes between MCHR1 and the mutated hormone, in which all amino acids but Cys7, Gly10, and Cys16 have in turn been replaced by alanine, highlight the relevance of Met8, Arg11, and Tyr13 for the MCH-induced chemical information transfer from the extracellular to the cytosolic domains, consistent with the experimental findings.[15] In fact, unlike the majority of the wild-type-like mutants of MCH, the complexes between MCHR1 and the MCH mutants at Met8, Arg11, and Tyr13, which are characterized by reduced ability to bind and activate the MCHR1, show some features of the active forms and some others of the inactive ones. In particular, in common with the inactive forms, these mutants share (1) the bend in helix 6, (2) the H-bond between D89(2.50) and N303(7.49), (3) the salt bridge between the E/DRY arginine and D79(2.40), and **SAS1** values below 100 Å^2 (Table II). We cannot, however, exclude the possibility that a fraction of the Arg11Ala mutant, which misses a key recognition point, might not reach the agonist binding site.

MD Simulations of the Empty Forms of MCHR2: Structural Features of the Inactive States

In the majority of the structures produced by all the short and long MD simulations of the empty MCHR2,

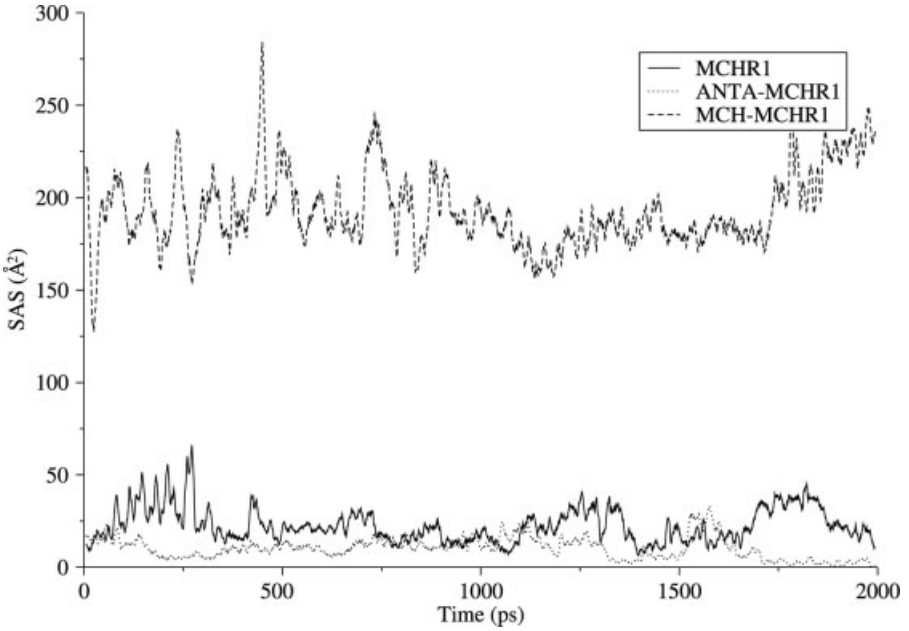

Fig. 4. Plot of the solvent accessible surface area (Å^2), computed over N76(2.37), R141(3.50), K153 (in I2), I247(6.26), and T251(6.30), versus time (ps), concerning the free (continuous line), antagonist-bound (dotted line), and MCH-bound (dashed line) forms of MCHR1. Lines have been smoothed by making running averages on 20 points, through the program XMGRACE.

TABLE II. Functional Data and Theoretical Descriptors Relative to the Complexes Between Truncated and Mutated Forms of MCH and the Two MCHRs

MCH variants[a]	% MCHR1 activation[b]	SAS1[c]	% MCHR2 activation[b]	SAS2[d]
MCH6-19	97	173.0	105	162.0
Asp1Ala	98	135.0	83	115.0
Phe2Ala	99	134.0	113	163.0
Asp3Ala	98	185.0	111	207.0
Met4Ala	99	158.0	116	140.0
Leu5Ala	97	124.0	110	149.0
Arg6Ala	72	83.0	85	98.0
Met8Ala	42	67.0	100	149.0
Leu9Ala	96	174.0	90	151.0
Arg11Ala	39	79.0	29	63.0
Val12Ala	93	156.0	108	177.0
Tyr13Ala	40	61.0	54	67.0
Arg14Ala	97	123.0	81	118.0
Pro15Ala	98	188.0	114	166.0
Trp17Ala	104	207.0	95	153.0
Gln18Ala	97	131.0	111	100.0
Val19Ala	98	145.0	112	150.0

[a]Truncated (MCH6-16) or mutant forms of MCH.
[b]Percentage of activation of the MCHR1 and MCHR2.[15]
[c]Solvent-accessible surface area (Å^2) computed over N76(2.37), R141(3.50), K153 (in I2), I247(6.26), and T251(6.30) in the complexes between the modified form of MCH and MCHR1 averaged over the 200 structures collected during the 100 ps of equilibrated MD simulation and minimized.
[d]Solvent accessible surface area (Å^2) computed over R131(3.50), A134(3.53), R143 (in I2), and V246(6.30) in the complexes between the modified form of MCH and MCHR2, averaged over the 200 structures collected during the 100 ps of equilibrated MD simulation and minimized.

R131(3.50) of the E/DRY motif is involved in salt bridge interactions with both D69(2.40) and the adjacent D130(3.49) (Table III, Figure 5). As for some of the highly conserved amino acids in the 7-helix bundle, (1) the interactions made by D79(2.50) include the H-bond with N302(7.49) of the NPxxY motif and van der Waals attractive interactions with N52(1.50); (2) W158(4.50) can be found involved in van der Waals attractive interaction with N74(2.45), V77(2.48), A119(3.38), and N154(4.46); (3) F260(6.44) is involved in persistent van der Waals attractive interactions with S121(3.40), S298(7.45), and N302(7.49); and (4) Y306(7.53) makes van der Waals attractive interactions with I55(1.53), C73(2.44), M252(6.36), and F313(7.60), as well as H-bonds with K65 in I1 (Table III). The majority of these interactions persist over the 2 ns time of the selected simulation. Another feature of the majority of the empty MCHR2 structures is a small bend at P266(6.50) (Fig. 5). This bend is smaller than that observed in the empty forms of MCHR1 due, at least in part, to the lack of the conserved tryptophan at position 6.48 (Figs. 1–3 and 5).

MD Simulations of the Agonist-Bound Forms of MCHR2: Structural Features of the Active States

In the majority of the MCH–MCHR2 complexes produced during the 44 short and 1 long MD simulations, the main orientation of the hormone is identical to that found in the complexes between the hormone and MCHR1.

We focus on a few relevant (according to the experimental evidence)[14,15] and persistent intermolecular interactions:

TABLE III. Intramolecular Interactions Involving Selected Amino Acid Side-Chains and Theoretical Indices Computed on the Average Minimized Structures of MCHR2

MCHR2	D79(2.50)[e]	D130(3.49)[e]	R131(3.50)[e]	N302(7.49)[e]	Y306(7.53)[e]	SAS2[f]
$FREE_{f100ps}$[a]	N52(1.50) **C120(3.39)** S299(7.46) **N302(7.49)**	**R131(3.50)** **W144**	D69(2.40) **D130(3.49)** L249(6.33)	**D79(2.50)** F260(6.44)	I55(1.53) **K65** C73(2.44) M252(6.36) F313(7.30)	5
$FREE_{f1000ps}$[b]	N52(1.50) **C120(3.39)** S299(7.46) **N302(7.49)**	**R131(3.50)** **R143**	D69(2.40) **D130(3.49)** L249(6.33)	**D79(2.50)** F260(6.44)	I55(1.53) **K65** C73(2.44) M252(6.36) F313(7.30)	7
$FREE_{l1000ps}$[c]	N52(1.50) C120(3.39) **N302(7.49)**	**R131(3.50)** **R143**	D69(2.40) **D130(3.49)** L249(6.33)	**D79(2.50)** F260(6.44)	I55(1.53) **K65** C73(2.44) M252(6.36) F313(7.30)	2
$FREE_{l100ps}$[d]	N52(1.50) **C120(3.39)** **N302(7.49)**	**R131(3.50)** **R143**	D69(2.40) **D130(3.49)** L249(6.33)	**D79(2.50)** F260(6.44)	I55(1.53) **K65** C73(2.44) M252(6.36) F313(7.30)	1
MCH-$bound_{f100ps}$[a]	**N116(3.35)** **N302(7.49)** **Y306(7.53)**	**R131(3.50)** W144	**D130(3.49)** A134(3.53) V246(6.30) L249(6.33)	**D79(2.50)** C120(3.39) Y306(7.53)	I55(1.53) I72(2.43) **D79(2.50)** N302(7.49)	221
MCH-$bound_{f1000ps}$[b]	**N116(3.35)** **A119(3.38)** **N302(7.49)** **Y306(7.53)**	**R131(3.50)** W144	**D130(3.49)** L135(3.54) V246(6.30) L249(6.33)	**N52(1.50)** **D79(2.50)** Y306(7.53)	**D79(2.50)** I123(3.42)	213
MCH-$bound_{l1000ps}$[c]	**N116(3.35)** **A119(3.38)** **N302(7.49)** **Y306(7.53)**	**R131(3.50)** W144 **R316(7.63)**	**D130(3.49)** A134(3.53) L135(3.54) V246(6.30) L249(6.33)	**N52(1.50)** **D79(2.50)** Y306(7.53)	I55(1.53) **D79(2.50)** I123(3.42)	188
MCH-$bound_{l100ps}$[d]	**N116(3.35)** **A119(3.38)** **N302(7.49)** **Y306(7.53)**	**R131(3.50)** W144 **R316(7.63)**	**D130(3.49)** A134(3.53) L135(3.54) V246(6.30) L249(6.33)	**N52(1.50)** **D79(2.50)** C120(3.39) Y306(7.53)	I55(1.53) **D79(2.50)** I123(3.42)	191

[a]Structures of the free (FREE) and agonist-bound (MCH-bound) forms of MCHR2, averaged over the 200 configurations collected during the first 100 ps of the selected 2 ns trajectories and minimized.
[b]Structures of the FREE and MCH-bound forms of MCHR2, averaged over the 2000 configurations collected during the first 1000 ps of the selected 2 ns trajectories and minimized.
[c]Structures of the FREE and MCH-bound forms of MCHR2, averaged over the 2000 configurations collected during the last 1000 ps of the selected 2 ns trajectories and minimized.
[d]Structures of the FREE and MCH-bound forms of MCHR2, averaged over the 200 configurations collected during the last 100 ps of the selected 2 ns trajectories and minimized.
[e]Amino acids involved in the selected intramolecular interactions. H-bonding interactions between the side chain atoms are highlighted in bold.
[f]Solvent accessible surface area ($Å^2$) computed over R131(3.50), A134(3.53), R143 (in I2), and V246(6.30).

1. In the first 100 ps, Arg6 is involved in H-bonds with T205(5.46) and Q271(6.55). The H-bond with Q271(6.55) is lost in the second half of simulation, whereas that with T205(5.46) occurs, even if not persistently, during the whole simulation. The interaction with Q271(6.55) is replaced by van der Waals attractive and/or H-bonding interactions with Y267(6.51).
2. Met8 is involved in interactions with V174 (in E2) and V170(4.62). The interaction with the former amino acid is persistent over the entire simulation time, whereas that with V170(4.62) occurs in the second half of simulation.
3. Arg11 is involved in persistent charge-reinforced H-bonds with both D113(3.32) and E182 (in E2), the latter being lost in the last steps of simulation, substituted by the H-bond with Q117(3.36) (Fig. 5). Furthermore, the functionally important arginine of the hormone is involved in van der Waals attractive interactions with I292(7.39) and Y296(7.43).
4. Tyr13 is essentially involved in persistent π-π coplanar interactions with F260(6.44) (Fig. 5).

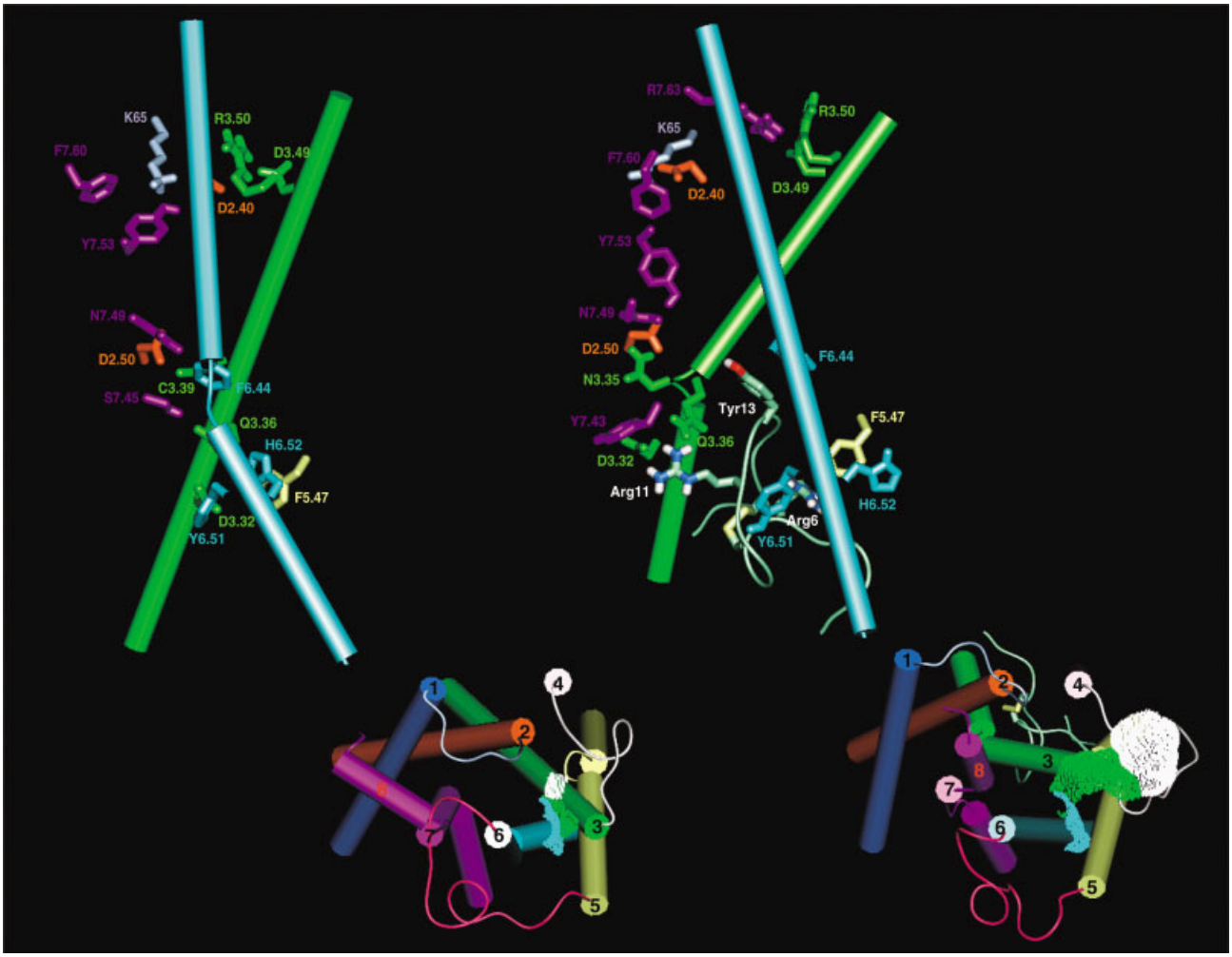

Fig. 5. Structures of the empty (**top and bottom left**) and MCH-bound (**top and bottom right**) forms of MCHR2 averaged over the 200 structures collected during the last 100 ps of the selected 2 ns trajectories and minimized. Coloring and amino acid labeling follow the criteria described in the legend to Figure 3. **Top view:** The models are viewed in a direction parallel to the membrane surface, the cytosolic side being at the top. Only helices 3 and 6 are shown, represented by cylinders. Details of selected intramolecular and intermolecular interactions are shown. **Bottom view:** The 7-helix bundle (represented by cylinders) and the 3 intracellular loops are shown from the intracellular side in a direction perpendicular to the membrane surface. The solvent-accessible surface computed over R131(3.50), A134(3.53), R143 (in I2), and V246(6.30) is represented by dots, colored according to the color of the corresponding amino acid.

The arrangement of the 7 helices in the MCH–MCHR2 complexes is different from that of the empty receptor (Fig. 5). In particular:

1. Helix 3 undergoes outward motions, being less tilted, slightly bent at N116(3.35), and shifted toward the cytosol. These shifts of helix 3 (as compared to the empty forms) are concurrent with outward shifts of helix 2, resulting in changes in helix1–helix2 and helix2–helix3 packing interactions. Such changes are marked, at least in part, by the establishment of almost persistent H-bonds between D79(2.50) and N116(3.35), and by the loss of the van der Waals attractive and ionic interactions found in the empty forms, respectively, between N52(1.50) and D79(2.50), and between D69(2.40) and R131(3.50), of the E/DRY motif (Table III, Fig. 5).
2. Helices 2 and 4 move apart significantly.
3. Helix 6 undergoes a clockwise rotation (seen from the intracellular side), lacking the bend at P266(6.50). These changes in helix 6 are concurrent with a change in the interaction pattern of F266(6.44), which is directed towards helix 5 instead of helix 7, as found in the empty receptor forms. Furthermore, S263(6.47) moves from helix 7, as found in the empty MCHR2, toward the core of the helix bundle, consistent with the experimental evidences on β_2-AR activation.[43]
4. Finally, another difference between the empty and MCH-bound forms of MCHR2 concerns the interaction pattern of Y306(7.53) of the NPxxY motif, which is no more engaged in interaction with F313(7.60), interacting with D79(2.50) and N302(7.49) (Table III, Fig. 5). The breakage of the interaction between Y306(7.53) and the conserved phenylalanine at position $i+7$, is

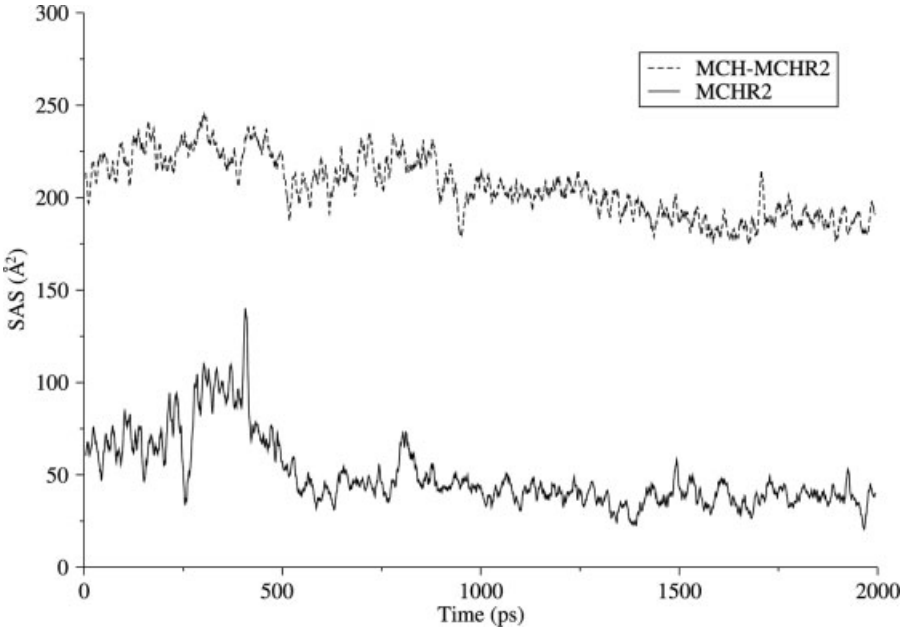

Fig. 6. Plot of the solvent-accessible surface area (Å^2) computed over R131(3.50), A134(3.53), R143 (in I2), and V246(6.30), versus time (ps), concerning the free (continuous line) and MCH-bound (dashed line) forms of MCHR2. Lines have been smoothed by making running averages on 20 points, through the program XMGRACE.

concurrent with a significant change in orientation of "helix 8," the main axis of this short helix being almost parallel to the membrane surface in the empty MCHR2 and becoming almost perpendicular in the MCH–MCHR2 complexes (Fig. 5). This structural change causes the approach of "helix 8" to the cytosolic extension of helix 3, marked by the salt bridge between R316(7.63) and D130(3.49), which occurs in the second half of simulation (Table III, Fig. 5). In fact, the distance between the α-carbon atoms of R316(7.63) and D130(3.49) is, respectively, 22.63 Å and 13.11 Å in the structures of the empty and agonist-bound MCHR2 averaged over the 200 configurations collected during the last 100 ps of the 2 ns trajectories.

An important feature that differentiates the empty from the hormone-bound MCHR2 is the opening of a solvent-accessible crevice in between I2 and the cytosolic extensions of helices 2, 3, and 6. This effect is described by the increased solvent accessibilities, as compared to the empty receptor forms, of selected amino acids. In fact, the solvent-accessible surface area computed over R131(3.50), A134(3.53), R143 (in I2), and V246(6.30) (i.e., **SAS2**, Table III) is significantly below 100 Å^2 in all the empty receptor forms collected over the different 2 ns trajectories, being significantly above 100 Å^2 in all the MCH-MCHR2 complexes constituting the 2 ns trajectory (Figs. 5 and 6).

Consistent with the experimental data,[15] MCH6-16 is able to induce perturbations in the interaction patterns of the highly conserved motifs similar to those induced by the full-length hormone. These perturbations are associated with a **SAS2** index above 100 Å^2 as well (Table II). Also, in this case, the transfer of the structural modification from the ligand-binding site to the cytosolic domains follows the establishment of the crucial intermolecular interactions involving D123(3.32) and F260(6.44) of the aromatic cluster in helix 6.

Molecular simulations of the complexes between MCHR2 and the mutated hormone, in which all amino acids but Cys7, Gly10, and Cys16 have been in turn replaced by alanine, suggest that the interaction between Tyr13 and F260(6.44) is a peculiarity of the high-affinity receptor states. In fact, this interaction is absent only in the Arg6Ala, Met9Ala, Arg11Ala, and Tyr13Ala mutants, which showed a dramatic loss of binding affinity, as compared to the wild-type hormone. Moreover, computations strengthen the relevance of Arg11 and Tyr13 for the MCH-induced chemical information transfer from the extracellular to the cytosolic domains, consistent with the experimental findings.[15] In fact, the Arg11Ala and Tyr13Ala mutants, characterized by reduced ability to bind and activate the MCHR2, share **SAS2** values below 100 Å^2 (Table II). In contrast, for all the other MCH mutants, characterized by a wild-type-like ability to activate MCHR2, the **SAS2** index is above 100 Å^2 (Table II). Apparently, the Gln18Ala mutant constitutes an exception to this trend. However, in this case, the opening of a solvent-accessible crevice in the cytosolic domains occurs but is not properly accounted for by the **SAS2** index.

DISCUSSION

In this study, an extensive computational analysis of the free, agonist-, and antagonist-bound forms of both subtypes 1 and 2 of the MCHR (i.e., MCHR1 and MCHR2) has

been carried out to gain insight into the mechanism of ligand-induced chemical information transfer from the extracellular to the intracellular sides of the receptors. We have essentially employed the same strategy that we used some years ago and again very recently to infer the structural modifications induced by functionally different ligands (agonists and antagonist) upon docking to the α_{1b}-adrenergic, m3-muscarinic, and 5-HT_{1A} serotonin receptors.[20,25,31] The approach consists of generating a large number of configurations of functionally different forms of the receptor [i.e., inactive (free and antagonist-bound) and active (agonist-bound)] by introducing perturbations in the input structure followed by short and long MD simulations. Comparative analyses of the receptor configurations are then carried out to find correlations between functional receptor state (i.e., inactive or active) and intermolecular and/or intramolecular interactions, focusing on the putative ligand-binding site and on highly conserved amino acids dislocated in distinct receptor portions. The comparative analyses are also aimed at defining theoretical indices able to distinguish between inactive and active receptor states.

The experimental data available on MCHRs and on homologous GPCRs have been employed in the different steps of the computational study (i.e., to build the receptor models, to help the selections of the most reliable average arrangements, to drive the ligand–receptor docking, and to support the mechanistic hypothesis on receptor activation as inferred from molecular simulations). The most relevant experimental information employed in the receptor model building is the crystal structures of rhodopsin.[3,19] In fact, the initial models of both MCHR1 and MCHR2 have been achieved, with acceptable reliability, by satisfying the structural restraints inferred from rhodopsin structure. In the step of the hormone–receptor docking, the structure of MCH has been employed, which had been previously achieved by NMR restraint-based MD.[18] The hormone–receptor docking has also profited by the information from (1) the invaluable results of alanine scanning mutagenesis, targeting almost all the amino acids in the hormone, as well as selected amino acids in the receptor, and (2) the results of binding and functional assays on synthetic modifications of the natural hormone.[14,15] The most relevant information from such experiments are that (1) the sequence Ac-Arg6-cyclo(S-S)(Cys^7-Met^8-Leu^9-Gly^{10}-Arg^{11}-Val^{12}-Tyr^{13}-Arg^{14}-Pro^{15}-Cys^{16})-NH_2 (i.e., MCH6-16) is the "active core" that is necessary for agonist binding and activation of both MCHR1 and MCHR2[15]; (2) within the "active core," Arg6, Met8, Arg11, and Tyr13, with prominence to the last two, are the few amino acids essential for MCH to properly bind and fully activate MCHRs[15]; and (3) the ionic interaction between Arg11 of the agonist and D123(3.32) of the receptor is an essential requirement for receptor recognition and activation by MCH.[14,15] Thus, based on the experimental evidence, the cyclic part of the hormone, despite its huge size, should dock into the core of the 7-helix bundle, where the key recognition point [i.e., D123(3.32)] is located. Interestingly, this aspartate corresponds to the aspartate that recognizes the cationic neurotransmitters in other subfamilies of GPCRs.[2] Other intriguing similarities between MCHRs and the cationic neurotransmitter GPCRs concern a cluster of aromatic amino acids at positions 6.44, 6.48, 6.51, and 6.52. MCHR2, however, lacks the tryptophan at 6.48 and holds a histidine at 6.52, instead of the conserved phenylalanine/tyrosine. Biochemical experiments on the α_{1b}-AR indicated that F6.51 is involved in interaction with the aromatic ring of epinephrine, whereas F6.52 performs interhelical interactions with amino acids in helix 5.[38] Taken together, these information suggest that the 10–amino acid cycle of MCH is instrumental for Arg11 and Tyr13 to reach the proper stereochemistry for establishing the key interactions with the receptor. These interactions might share some commonalties with those that are necessary for cationic neurotransmitters to activate their target receptors.

Despite their structural differences, MCHR1 and MCHR2, however, share the structural hallmarks of the inactive and active states. Indeed, the extensive analysis of receptor configurations suggests that the receptor portions close to the E/DRY and NPxxY motifs in helices 3 and 7, respectively, are particularly susceptible to undergo structural modification in response to agonist binding. The interaction patterns involving the members of the two highly conserved motifs share significant commonalties in the inactive forms of MCHR1 and MCHR2. Indeed, the majority of the empty forms of both MCHR1 and MCHR2 are characterized by salt bridges between R3.50 of the E/DRY motif, and both D2.40 and the adjacent D3.49 (Tables I and III, Figs. 3 and 5). The interaction with D2.40 is a peculiarity of MCHRs, which lack the anionic amino acid at position 6.30, found as the interhelical interaction partner of R3.50 in rhodopsin structure[3] and suggested to be involved in an equivalent interaction in the inactive states of the α_{1b}-AR,[28,29] β_2-AR,[44] 5-HT_{1A}, and 5-HT_{2A} serotonin receptors[31,45,46] and the lutropin receptor.[30] The two salt bridge interactions involving R3.50 in the empty forms of the two MCHRs link together the cytosolic ends of helices 3 and 2 (Figs. 3 and 5). In both receptors, the aliphatic chain of R3.50 is also involved in van der Waals attractive interactions with the amino acids at positions 6.30 and 6.33, indicative of the close packing between the cytosolic ends of helices 3 and 6 (Figs. 3 and 5). Such interactions of R3.50, which also characterize almost all the simulated complexes between the synthetic antagonist T-22629632 and MCHR1 (Scheme 1, Table I, and Fig. 3), are always concurrent with the presence of interactions between the tyrosine of the NPxxY motif and F7.60, in "helix 8." Moving from the cytosolic side to the transmembrane portion of the helix bundle, an interaction that characterizes the inactive forms of the two MCHRs is the H-bond between D2.50 and N7.49 of the NPxxY motif (Tables I and III, Figs. 3 and 5). A serine at position 7.46 can be additionally found involved in H-bond with D2.50, even if less frequently than N7.49. These interactions constitute a structural link between helices 2 and 7. However, we do not exclude the possibility that one or more water molecules might mediate the H-bonds involv-

ing these polar conserved amino acids. This is also suggested by the advances in determination of rhodopsin structure.[42]

The interaction patterns that characterize the E/DRY and NPxxY motifs in the inactive receptor states are perturbed following the establishment of peculiar intermolecular interaction between the natural agonist MCH and both MCHRs. In particular, for the MCH–MCHR1 complex, these interactions include (1) the charge-reinforced H-bond between Arg11 and D123(3.32), consistent with the experimental evidence,[14] (2) interactions between Tyr13 and one or more members of the aromatic cluster in helix 6, such as W269(6.48) and/or Y272(6.51), and (3) van der Waals attractive interactions between Arg11 and both I292(7.39) and Y296(7.43). It is worth noting that in the majority of the simulated complexes, Arg11 donates a charge-reinforced H-bond not only to D123(3.32) but also to an additional acceptor that is frequently Q127(3.36) or Y272(6.51). The establishment of such intermolecular interactions between MCH and MCHR1 causes changes in the helix 1–helix 2, helix 2–helix 3, helix 2–helix 4, and helix 2–helix 7 packing, marked, at least in part, by the establishment of interactions between D89(2.50) and both N125(3.35) and T129(3.40), as well as by the loss of the interactions, found in the empty and antagonist-bound forms of MCHR1 between N84(2.45) and W168(4.50), and between D89(2.50) on one side and N58(1.50), S304(7.46), and N307(7.49) on the other (Table I, Fig. 3). Furthermore, the interactions between MCH and the members of the aromatic cluster in helix 6 are concurrent with a change in orientation of the W269(6.48) side-chain, which becomes oriented toward helix 5 instead of helix 7, as found in the inactive receptor forms (Fig. 3). The same happens to F265(6.44), which follows the motion of W269(6.48). The agonist-induced rearrangement of the members of the aromatic cluster in helix 6 is concurrent with a significant reduction in the bend at P271(6.50), as compared to the inactive forms (Fig. 3). Moving into the cytosolic domains, the agonist-bound forms are characterized by a destabilization of the van der Waals attractive interaction found in the inactive forms between Y311(7.53) and F318(7.60), the NPxxY tyrosine being directed toward helices 3 and 6, interacting with the amino acids at positions 3.42, 3.43, and 6.40 (Table I). Such changes involving the NPxxY motif are concurrent with the approaching of "helix 8" to the cytosolic extension of helix 3 (Fig. 3). Another feature that characterizes the MCH–MCHR1 complexes is the breakage of the salt bridge found in the free and antagonist-bound receptor forms between R141(3.50) of the E/DRY motif and D79(2.40) (Fig. 3). The H-bonding contribution to the interaction between the E/DRY arginine and the adjacent aspartate is also broken in most of the MCH–MCHR1 complexes (Table I). The MCH-induced rearrangements of the cytosolic domains is concurrent with the opening of a solvent-accessible crevice in between I2 and the cytosolic ends of helices 2, 3, and 6. Such structural change is properly described by the solvent-accessible surface area computed over N76(2.37), R141(3.50), K153 (in I2), I247(6.26), and T251(6.30) (i.e., **SAS1**, Table I). This index is always significantly below 100 Å^2, frequently close to 0 Å^2, in the empty and antagonist-bound forms, being persistently and significantly above 100 Å^2 in those MCH–MCHR1 complexes, in which both Arg11 and Tyr13 accomplish the peculiar interactions with the receptor (Table I, Figs. 3 and 4).

Simulations of the MCH–MCHR2 complexes have shown that the establishment of (1) H-bonds between Arg6 and Q271(6.55) or Y267(6.51), (2) charge-reinforced H-bonds between Arg11 and both D123(3.32) and E182 (in E2) [the latter is substituted by Q117(3.36) in the latest steps of simulation], (3) π-π coplanar interactions between Tyr13 and F265(6.44), and (4) van der Waals attractive interactions between Arg11 and both I292(7.39) and Y296(7.43) is concurrent with the breakage of the interactions between R131(3.50) of the E/DRY motif and D79(2.40), and between Y311(7.53), of the NPxxY motif and F318(7.60), as well as with a change in orientation of "helix 8," which approaches the cytosolic end of helix 3 (Fig. 5). Similar to the MCH–MCHR1 complexes in the MCH-MCHR2 complexes the structural changes in the cytosolic domains are concurrent with the opening of a solvent-accessible crevice in between I2 and the cytosolic extensions of helices 2, 3, and 6, an effect that is properly described by the solvent-accessible surface area computed over R131(3.50), A134(3.53), R143 (in I2) and V246(6.30) (**SAS2**, Table III). This index is indeed significantly below 100 Å^2, most frequently close to 0 Å^2 in the empty receptor forms, and significantly above 100 Å^2 in the agonist-bound receptor forms (Table III, Figs. 5 and 6).

Consistent with the experimental findings,[15] molecular simulations of the complexes between the MCH6-16 truncated peptide and either MCHR1 or MCHR2 have shown that the establishment of (1) charge-reinforced H-bonds and van der Waals attractive interactions between Arg11 and amino acids in helices 3 and 7, and (2) van der Waals attractive interactions between Tyr13 and W6.48 or F6.44 of the aromatic cluster in helix 6 is concurrent with changes in the interaction patterns of the E/DRY and NPxxY motifs, as well as with the opening of a solvent-accessible crevice in the cytosolic domains, similar to the receptor complexes with the full-length peptide (Table II).

The relevance of D3.32 of the aromatic cluster in helix 6 and of the amino acids at positions 7.39 and 7.43 in the transfer of the chemical information from the extracellular to the cytosolic domains is corroborated by the results of molecular simulations of the complexes between the mutants forms of MCH and either MCHR1 or MCHR2 (Table II). In fact, the Arg11Ala and Tyr13Ala mutants of MCH, which are no more able to accomplish the proper interactions with the amino acids on helices 3 and 7 and/or with the members of the aromatic cluster in helix 6, share some features of the inactive forms, including the **SAS1** and **SAS2** indices below 100 Å^2 (Table II).

Overall, the inferences from our study are consistent with the results of biochemical experiments demonstrating that GPCRs of the rhodopsin family can be activated through Zn^+ coordination between metal-ion binding residues located at positions 3.32 and 7.39.[47,48] The finding

that the metal-ion–mediated link between such points on helices 3 and 7 is able to induce only partial agonism[47,48] is explained by the results of the computational modeling herein presented, suggesting that additional interactions between the agonist and members of the aromatic cluster in helix 6 are required for the hormone to induce peculiar structural changes in the cytosolic domains as compared to the empty receptor forms. Further convergent results concern the structural features of the antagonist-bound forms of MCHR1, which are similar to those of the empty receptor forms, in part because the ligand is not able to perturb the aromatic cluster in helix 6 (Fig. 3). The functional importance of the aromatic cluster in helix 6 has been previously suggested by computations and experiments on the D2-dopamine receptor,[49] the α_{1b}-AR,[25] and the 5-HT_{1A} serotonin receptor.[31]

All together, the inferences from computations and experiments suggest that the essential requirements for the agonist to perturb the peculiar features of the inactive forms of MCHRs are to accomplish the electrostatic interaction with the binding-site aspartate and to perform van der Waals attractive interactions with one of more members of the aromatic cluster in helix 6. These interactions involve essentially 2 of the 19 amino acids that constitute the hormone. In this respect, the precise details of the binding interactions, which involve the whole hormone and can differ even within the same MD trajectory, are not relevant. In this scenario, the few critical interactions needed for the huge MCH or for the small serotonin to transfer the chemical information from the extracellular to the intracellular domains of their target receptors are overlapping (this work and Seeber et al.[31]).

In summary, the results of this study strengthen the hypothesis that the differences between inactive and active states of MCHRs involve the receptor portions close to the E/DRY and NPxxY motifs, with prominence to the cytosolic extensions of helices 2, 3, 6, and 7. In fact, an increase in solvent accessibility (as compared to the inactive forms) of selected amino acids in the cytosolic extensions of helices 2, 3, and 6, and in I2, characterize the agonist-bound forms of both MCHR1 and MCHR2. These results are consistent with the results of crosslinking, spin-labeling, and scanning-accessibility experiments on rhodopsin (reviewed by Meng and Bourne[50]). In fact, mapping these experimental data onto the rhodopsin structure suggests that activation by light opens a cleft at the cytoplasmic end of the helix bundle with separation of transmembrane helices 3 and 6, and increased exposure of the inner faces of helices 2, 3, 6, and 7.[50] The results of our study are also consistent with recent experimental evidence on rhodopsin activation, indicating that the $NPxxY(x)_{5,6}F$ and E/DRY motifs provide, in concert, a dual control of the activating structural changes in the photoreceptor.[51] Whether the E/DRY and NPxxY motifs work in concert in MCHR activation, as suggested by our computational analysis, should be experimentally probed. The amino acids that mark the opening of the solvent-accessible crevice in the agonist-bound forms of the two MCHRs lie almost at the same positions in the two receptors, suggestive of potential roles of such receptor portions in G-protein recognition.

Another remarkable, peculiar feature of the active forms of both MCHRs, particularly of MCHR2, is the approaching of "helix 8" to the cytosolic extension of helix 3. This effect is properly accounted for by the significant reduction in distance between the α-carbon atoms of R7.63 and D3.49. Despite the fact that the electrostatic interaction between R7.63 and D3.49 may have been overestimated due to the absence of the screening effect of water, it is also true that the approaching of helix 8 to the cytosolic extension of helix 3 is a feature of the active forms of MCHRs and not of the nonactive ones. Active and nonactive forms of both receptors have been simulated by using the same computational setup. These structural changes, suggestive of increased flexibility of helices 7 and 8, are consistent with the experimental evidences that a disulfide bridge is allowed to form between the amino acids at positions 7.63 and 3.55 in the light-activated states of rhodopsin, and not in the dark state.[50,52]

The results of computations have highlighted the involvement of D2.40 at the cytosolic end of helix 2 in the most significant structural differences between active and inactive states of both MCHRs. Whether this aspartate plays a relevant role in MCHR function awaits experimental assessment.

The computational analysis in this study has highlighted the following amino acids in the extracellular half of the receptor: D3.32, Q3.36, F6.44, W6.48, Y6.51, I7.39, and Y7.43, which may be involved in agonist binding and/or in the agonist-induced receptor transition from the inactive to the active states. The importance of D3.32 for MCH-induced MCHR1 activation has been already proved,[14] whereas it would be interesting to investigate the role of the aromatic amino acids in such list.

A significant reduction in the bend at P(6.50), as compared to the empty and the antagonist-bound receptor forms, is one of the features shared by the agonist-bound forms (Figs. 3 and 5). These results, agree with the computer simulation and experiment-based hypothesis that GPCR activation would significantly diminish the kink at P6.50.[53] The role of the highly conserved P6.50 in the MCHR function has yet to be investigated by site-directed mutagenesis experiments.

The computational modeling presented in this article is based upon approximations and simplifications. The major problems are associated with the rough evaluation of the electrostatic energies, including the dielectric constants that represent the effect of the protein environment.[54] One consequence of the lack of proper screening effect of the solvent is an overall overestimation of the water-exposed salt bridges and charge-reinforced H-bonding interactions. Despite these drawbacks, the extensive comparative analysis in this study aimed at inferring similarity/differences within the same approximations has been able to infer a few significant structural features that differentiate the inactive from the active receptor states.

The results of this study provide useful suggestions for new experiments aimed at elucidating GPCR function.

ACKNOWLEDGMENTS

We are very grateful to Dr. Piero Amodeo for the *ad hoc* setup of the Linux Clusters employed for MD simulations.

REFERENCES

1. Bockaert J, Pin JP. Molecular tinkering of G protein-coupled receptors: an evolutionary success. EMBO J 1999;18:1723–1729.
2. Gether U. Uncovering molecular mechanisms involved in activation of G protein-coupled receptors. Endocr Rev 2000;21:90–113, and references therein.
3. Palczewski K, Kumasaka T, Hori T, Behnke CA, Motoshima H, Fox BA, Le Trong I, Teller DC, Okada T, Stenkamp RE, Yamamoto M, Miyano M. Crystal structure of rhodopsin: a G protein-coupled receptor. Science 2000;289:739–745.
4. Bachner D, Kreienkamp H, Weise C, Buck F, Richter D. Identification of melanin concentrating hormone (MCH) as the natural ligand for the orphan somatostatin-like receptor 1 (SLC-1). FEBS Lett 1999;457:522–524.
5. Chambers J, Ames RS, Bergsma D, Muir A, Fitzgerald LR, Hervieu G, Dytko GM, Foley JJ, Martin J, Liu W-S, Park J, Ellis C, Ganguly S, Konchar S, Chuderay J, Leslie R, Wilson S, Sarau HM. Melanin-concentrating hormone is the cognate ligand for the orphan G-protein-coupled receptor SLC-1. Nature 1999;400:261–265.
6. Lembo P, Grazzini E, Cao J, Hubatsch D, Pelletier M, Hoffert C, St-Onge S, Pou C, Labrecque J, Groblewski T, O'Donnell D, Payza K, Ahmad S, Walker P. The receptor for the orexigenic peptide melanin-concentrating hormone is a G protein-coupled receptor. Nat Cell Biol 1999;1:267–271.
7. Saito Y, Nothacker H-P, Wang Z, Lin SHS, Leslie F, Civelli O. Molecular characterization of the melanin-concentrating hormone receptor. Nature 1999;400:265–269.
8. Saito Y, Nothacker HP, Civelli O. Melanin-concentrating hormone receptor: an orphan receptor fits the key. Trends Endocrinol Metab 2000;11:299–303.
9. Boutin JA, Suply T, Audinot V, Rodriguez M, Beauverger P, Nicolas J-P, Galizzi J-P, Fauchere J-L. Melanin-concentrating hormone and its receptors: state of the art. Can J Physiol Pharmacol 2002;80:388–395, and references therein.
10. Qu D, Ludwig DS, Gammeltoft S, Piper M, Pelleymounter MA, Cullen MJ, Mathes WF, Przypek J, Kanarek R, Maratos-Flier E. A role for melanin-concentrating hormone in the central regulation of feeding behaviour. Nature 1996;380:243–247.
11. Mori M, Harada M, Terao Y, Sugo T, Wanabe T, Shimomura Y, Abe M, Shintani Y, Onda H, Nishimura O, Fujino M. Cloning of a novel G protein-coupled receptor, SLT, a subtype of the melanin-concentrating hormone receptor. Biochem Biophys Res Commun 2001;283:1013–1018.
12. Hill J, Duckworth M, Murdock P, Rennie G, Sabido-David C, Ames RS, Szekeres P, Wilson S, Bergsma DJ, Gloger IS, Levy DS, Chambers JK, Muir AI. Molecular cloning and functional characterization of MCH2, a novel human MCH receptor. J Biol Chem 2001;276:20125–20129.
13. Sailer AW, Sano H, Zeng Z, McDonald TP, Pan J, Pong SS, Feighner SD, Tan CP, Fukami T, Iwaasa H, Hreniuk DL, Morin NR, Sadowsky SJ, Nossoughi R, Ito M, Ito M, Bansal A, Ky B, Figueroa DJ, Jiang Q, Austin CP, MacNeil DJ, Ishihara A, Ihara M, Kanatani A, Van der Ploeg LHT, Howard AD, Liu Q. Identification and characterization of a second melanin-concentrating hormone receptor, MCH-2R. Proc Natl Acad Sci USA 2001;98:7564–7569.
14. MacDonald D, Mugolo N, Zhang R, Durkin JP, Yao X, Strader CD, Graziano MP. Molecular characterization of the melanin-concentrating hormone/receptor complex: identification of critical residues involved in binding and activation. Mol Pharmacol 2000;58:217–225.
15. Bednarek MA, Feighner SD, Hreniuk DL, Palyha OC, Morin NR, Sadowski SJ, MacNeil DJ, Howard AD, van der Ploeg LHJ. Short segment of human melanin-concentrating hormone that is sufficient for full activation of human melanin-concentrating hormone receptors 1 and 2. Biochemistry 2001;40:9379–9386.
16. Brown DW, Campbell MM, Kinsman RG, White PD, Moss CA, Osguthorpe DJ, Paul PK, Baker BI. Melanin-concentrating hormone: a structural and conformational study based on synthesis, biological activity, high-field NMR, and molecular modeling techniques. Biopolymers 1990;29:609–622.
17. Paul PKC, Dauber-Osguthorpe P, Campbell MM, Brown DW, Kinsman RG, Moss C, Osguthorpe DJ. Accessible conformations of melanin-concentrating hormone: a molecular dynamics approach. Biopolymers 1990;29:623–637.
18. Vitale RM, Zaccaro L, Di Blasio B, Fattorusso R, Isernia C, Amodeo P, Pedone C, Saviano M. Conformational features of human melanin-concentrating hormone: a NMR and computational analysis. ChemBioChem 2003;4:73–81.
19. Teller DC, Okada T, Behnke CA, Palczewski C. Advances in determination of a high resolution three dimensional structure of rhodopsin, a model of G protein coupled receptors (GPCRs). Biochemistry 2001;40:7761–7772.
20. Fanelli F, Menziani MC, De Benedetti PG. Computer simulations of signal transduction mechanism in α_{1b}-adrenergic and m3-muscarinic receptors. Prot Eng 1995;8:557–564.
21. Scheer A, Fanelli F, Costa T, De Benedetti PG, Cotecchia S. Constitutively active mutants of the α_{1B}-adrenergic receptor: role of highly conserved polar amino acids in receptor activation. EMBO J 1996;15:3566–3578.
22. Scheer A, Fanelli F, Costa T, De Benedetti PG, Cotecchia S. The activation process of the α_{1B}-adrenergic receptor: potential role of protonation and hydrophobicity of a highly conserved aspartate. Proc Natl Acad Sci USA 1997:94;808–813.
23. Fanelli F, Menziani MC, Scheer A, Cotecchia S, De Benedetti PG. Ab initio modeling and molecular dynamics simulation of the α_{1b}-adrenergic receptor activation. Methods Companion to Methods Enzymol 1998;14:302–317, and references therein.
24. Fanelli F, Menziani MC, Scheer A, Cotecchia S, De Benedetti PG. Theoretical study of the electrostatically driven step of receptor-G protein recognition. Proteins 1999;37:145–156.
25. Fanelli F, Menziani MC, Scheer A, Cotecchia S, De Benedetti PG. Theoretical study on receptor/G protein recognition: new insights into the mechanism of the α_{1b}-adrenergic receptor activation. Int J Quant Chem 1999;73:71–83.
26. Fanelli F, Barbier P, Zanchetta D, De Benedetti PG, Chini B. Activation mechanism of human oxytocin receptor: a combined study of experimental and computer-simulated mutagenesis. Mol Pharmacol 1999;56:214–225.
27. Fanelli F. Theoretical study on mutation-induced activation of the luteinizing hormone receptor. J Mol Biol 2000;296:1333–1351.
28. Greasley PJ, Fanelli F, Scheer A, Abuin L, Nenniger-Tosato M, De Benedetti PG, Cotecchia S. Mutational and computational analysis of the α_{1b}-adrenergic receptor: involvement of basic and hydrophobic residues in receptor activation and G protein coupling. J Biol Chem 2001;276:6485–6494.
29. Greasley PJ, Fanelli F, Rossier O, Abuin L, Cotecchia S. Mutagenesis and modelling of the α_{1b}-adrenergic receptor highlight the role of helix3/helix 6 interface in receptor activation. Mol Pharmacol 2002;61:1–8.
30. Angelova K, Fanelli F, Puett D. Engineered and simulated mutations in transmembrane helices 6 and 7 of the lutropin receptor: a model for constitutive and ligand-mediated receptor activation. J Biol Chem 2002;277:32202–32213.
31. Seeber M, De Benedetti PG, Fanelli F. Molecular dynamics simulations of the ligand-induced chemical information transfer in the 5-HT_{1A} receptor. J Chem Inf Comput Sci 2003;43:1520–1531.
32. Takekawa S, Asami A, Ishihara Y, Terauchi J, Kato K, Shimomura Y, Mori M, Murakoshi H, Kato K, Suzuki N, Nishimura O, Fujino M. T-226296: a novel, orally active and selective melanin-concentrating hormone receptor antagonist. Eur J Pharmacol 2002;438:129–135.
33. Sali A, Blundell TL. Comparative protein modelling by satisfaction of spatial restraints. J Mol Biol 1993;234:779–815.
34. Brooks BR, Bruccoleri RE, Olafson BD, States DJ, Swaminathan S, Karplus M. CHARMM: a program for macromolecular energy, minimization and dynamics calculations. J Comput Chem 1983;4:187–217.
35. MacKerell AD Jr, Bashford D, Bellott M, Dunbrack RL Jr, Evanseck JD, Field MJ, Fischer S, Gao J, Guo H, Ha S, Joseph-McCarthy D, Kuchnir L, Kuczera K, Lau FTK, Mattos C, Michnick S, Ngo T, Nguyen DT, Prodhom B, Reiher WE III, Roux B, Schlenkrich M, Smith JC, Stote R, Straub J, Watanabe M, Wiorkiewicz-Kuczera J, Yin D, Karplus M. All-atom empirical

potential for molecular modeling and dynamics studies of proteins. J Phys Chem B 1998;102:3586–3616.
36. Ballesteros JA, Weinstein H. Integrated methods for the construction of three-dimensional models and computational probing of structure-function relations in G protein-coupled receptors. Methods Neurosci 1995;25:366–428.
37. Farrens DL, Altenbach C, Yang K, Hubbell WL, Khorana HG. Requirement of rigid-body motion of transmembrane helices for light activation of rhodopsin. Science 1996;274:768–770.
38. Chothia C, Lesk AM. The relation between the divergence of sequence and structure in proteins. EMBO J 1986;5:823–826.
39. Chen S, Xu M, Lin F, Lee D, Riek P, Graham RM. Phe^{310} in transmembrane VI of the α_{1b}-adrenergic receptor is a key switch residue involved in activation and catecholamine ring aromatic bonding. J Biol Chem 1999;274:16320–16330.
40. Cavalli A, Fanelli F, Taddei C, De Benedetti PG, Cotecchia S. Amino acids of the α_{1B}-adrenergic receptor involved in agonist binding: further differences in docking catecholamines to receptor subtypes. FEBS Lett 1996;399:9–13.
41. Dewar MJS, Zoebisch EG, Healey EF, Stewart JJP. AM1: a new general purpose quantum mechanical molecular model. J Am Chem Soc 1985;107:3902–3909.
42. Okada T, Fujiyoshi Y, Silow M, Navarro J, Landau EM, Shichida Y. Functional role of internal water molecules in rhodopsin revealed by X-ray crystallography. Proc Natl Acad Sci USA 2002;99:5982–5987.
43. Ghanouni P, Steenhuis JJ, Farrens DL, Kobilka BK. Agonist-induced conformational changes in the G-protein-coupling domain of the β_2 adrenergic receptor. Proc Natl Acad Sci USA 2001;98:5997–6002.
44. Ballesteros JA, Jensen AD, Liapakis G, Rasmussen SG, Shi L, Gether U, Javitch JA. Activation of the β_2-adrenergic receptor involves disruption of an ionic lock between the cytoplasmic ends of transmembrane segments 3 and 6. J Biol Chem 2001;276:29171–29177.
45. Shapiro DA, Kristiansen K, Weiner DM, Kroeze WK, Roth BLJ. Evidence for a model of agonist induced activation of 5-hydroxytryptamine 2A serotonin receptors that involves the disruption of a strong ionic interaction between helices 3 and 6. J Biol Chem 2002;277:11441–11449.
46. Visiers I, Ebersole B, Dracheva S, Ballesteros J, Sealfon SC, Weinstein H. Structural motifs as functional microdomains in G protein coupled receptors: energetic considerations in the mechanism of activation of the serotonin 5-HT$_{2A}$ receptor by disruption of the ionic lock of the arginine cage. Int J Quant Chem 2002;88:65–75.
47. Elling CE, Thirstrup K, Holst B, Schwartz TW. Conversion of agonist site to metal-ion chelator site in the β_2-adrenergic receptor. Proc Natl Acad Sci USA 1999;96:12322–12327.
48. Holst B, Elling CE, Schwartz TW. Partial agonism through a zinc-ion switch constructed between transmembrane domains III and VII in the tachykinin NK$_1$ receptor. Mol Pharmacol 2000;58:263–270.
49. Javitch JA, Ballesteros JA, Weinstein H, Chen J. A cluster of aromatic residues in the sixth membrane-spanning segment of the dopamine D$_2$ receptor is accessible in the binding-site crevice. Biochemistry 1998;37:998–1006.
50. Meng EC, Bourne H. Receptor activation: what does rhodopsin structure tell us? Trends Pharmacol Sci 2001;22:587–593, and references therein.
51. Fritze O, Filipek S, Kuksa V, Palczewski K, Hofmann KP, Ernst OP. Role of the conserved NPxxY(x)$_{5,6}$F motif in the rhodopsin ground state and during activation. Proc Natl Acad Sci USA 2003;100:2290–2295.
52. Yu H, Kono M, Oprian DD. State dependent disulfide cross-linking in rhodopsin. Biochemistry 1999;38:12028–12032.
53. Sansom MSP, Weinstein H. Hinges, swilves and switches: the role of prolines in signalling via transmembrane α-helices. Trends Pharm Sci 2000;21:445–451, and references therein.
54. Schutz CN, Warshel A. What are the dielectric "constants" of proteins and how to validate electrostatic models? Proteins 2001;44:400–417, and references therein.